TECHNICAL REPORT 1942
September 2006

A Pareto Approach to Lossy Matching

J. C. Allen
D. Arceo

SSC San Diego
San Diego, CA 92152-5001

Report Documentation Page

Form Approved
OMB No. 0704-0188

1. REPORT DATE	2. REPORT TYPE	3. DATES COVERED
SEP 2006		**00-00-2006 to 00-00-2006**

4. TITLE AND SUBTITLE	5a. CONTRACT NUMBER
A Pareto Approach to Lossy Matching	5b. GRANT NUMBER
	5c. PROGRAM ELEMENT NUMBER
6. AUTHOR(S)	5d. PROJECT NUMBER
	5e. TASK NUMBER
	5f. WORK UNIT NUMBER
7. PERFORMING ORGANIZATION NAME(S) AND ADDRESS(ES) **Space and Naval Warfare Systems Center,53560 Hull Street,San Diego,CA,92152-5001**	8. PERFORMING ORGANIZATION REPORT NUMBER
9. SPONSORING/MONITORING AGENCY NAME(S) AND ADDRESS(ES)	10. SPONSOR/MONITOR'S ACRONYM(S)
	11. SPONSOR/MONITOR'S REPORT NUMBER(S)

12. DISTRIBUTION/AVAILABILITY STATEMENT
Approved for public release; distribution unlimited

13. SUPPLEMENTARY NOTES
The original document contains color images.

14. ABSTRACT

15. SUBJECT TERMS

16. SECURITY CLASSIFICATION OF:			17. LIMITATION OF ABSTRACT	18. NUMBER OF PAGES	19a. NAME OF RESPONSIBLE PERSON
a. REPORT **unclassified**	b. ABSTRACT **unclassified**	c. THIS PAGE **unclassified**		**61**	

Acknowledgments

The authors thank Robert S. Abramo of SPAWAR Systems Center San Diego for providing the photographs of the Surface Probe shown in Figures 1 and 2 of this report. The photographs are from Abramo's 2005 report Electrical Evaluation and Comparison of Five HF Receive Antenna Over 150 kHz–30 MHz, which was prepared for PEI-C4I & Space, PMW-180, Space and Naval Warfare Systems Command.

Executive Summary

This report originated in the In-House Laboratory Independent Research Program of SPAWAR Systems Center San Diego and continues the migration of H^∞ Engineering into fleet applications.

As more communication systems are installed and radar cross-section requirements become stricter, shipboard space has become extremely limited and new antenna designs must be considered. As antenna size is reduced, a tradeoff between efficiency and bandwidth is forced. This report offers a multiobjective solution where transducer power gain is traded to reduce the large reflection at the feed of the antenna. Although lossy matching is an anathema for standard antenna matching, trading gain against reflection is rational design objective for a small antenna—provided the corresponding Pareto front can be computed.

This report offers several techniques to compute the Pareto front for a given lossy topology—random sampling, orbit techniques based on lossless matching, and the adaptation of the H^∞ techniques. These Pareto front computations readily adapt to other lossy matching tradeoffs and offer a general approach to lossy matching.

Contents

List of Figures

1 Why Lossy Matching?

The U.S. Navy is presently working on new electrically small antennas for high-frequency (HF) communications. One such antenna is the Surface Probe being developed by SPAWAR Systems Center San Diego, Code 285. The Surface Probe is approximately 10 feet by 2 feet and is shown in Figure 1. For illustration, the wavelength at 2 MHz is approximately 492 feet, while the Surface Probe is only 10-feet long.

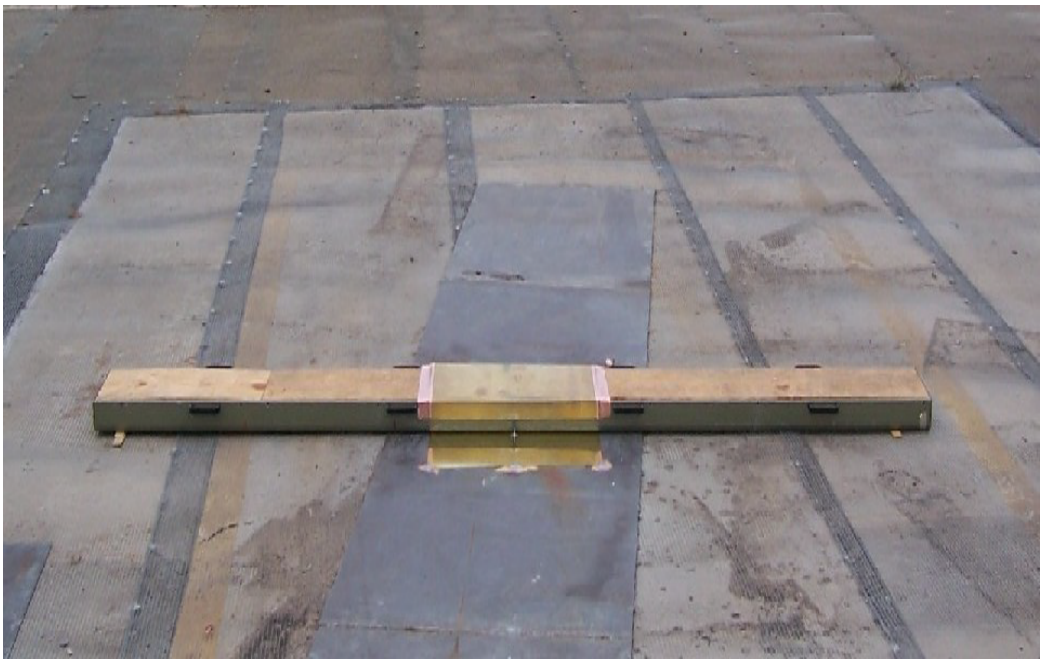

Figure 1: The 10-foot Surface Probe.

The Surface Probe is constrained in volume and its properties determine the efficiency of the antenna. Therefore, the properties of the Surface Probe limit its bandwidth by the known bandwidth efficiency product. Given that the antenna parameters are set—could a lossy matching network be designed to meet the bandwidth requirements? By adding loss, more bandwidth may be acquired at a cost in the transducer power gain of the matching network. This question motivates this report's exploration of lossy matching.

Several modifications of the Surface Probe were tested to improve matching. One modification added extra cable to change the phase of the antenna

and was called the "loop with cable." However, the antenna impedance used was measured directly from the feed point shown in Figure 2, and is therefore called the Loop Without Cable (LWC).

Figure 2: Closeup of the feed point in the Surface Probe.

Section 2 starts the analysis of the LWC antenna by computing best bounds for lossless matching for benchmarks. Section 3 offers optimal lossless ladders that later serve as computational testbeds for the lossy matching. Section 4 carefully sets out the optimization problem for lossy matching:

- Maximize power transfered to the antenna
- Minimize power reflected from the antenna

to avoid falling for the bogus solution of Section 5. Section 6 undertakes the numerical solution of this multiobjective problem and shows the limitations of random sampling to compute the best design curves where gain is traded against reflected power. Section 7 offers the orbit approach as one method for a fast computation of these design curves. Section 8 bounds the design

curves based on H^∞ techniques. These bounds offer the antenna designer a target region of optimal performance. Section 9 plots the design curves in an engineering context of transmission loss and voltage standing wave ratio (VSWR). Section 10 concludes by comparing the H^∞ bounds and the design curves. Research opportunities are made explicit. Thus, the antenna designer can find a collection of lossy matching techniques and research opportunities in this report.

2 Lossless Matching Bounds

Recent developments in H^∞ Engineering allow the antenna designer to compute the best possible match—independent of circuit topology [9], [10], [11], [17]. Accordingly, *lossless* matching performance of the LWC antenna is presented in this section to benchmark the forthcoming *lossy* matching designs.

Figure 3 presents the standard H^∞ matching plot that shows VSWR as a function degree d of the lossless matching circuit [1], [2]. The dotted black line at the VSWR of 34.5 marks the unmatched VSWR of the LWC over 2 to 9 MHz. The red patch marks the H^∞ bound that is the best possible match attainable by any lossless 2-port and corresponds to the degree d goes to infinity. Equivalently, the H^∞ bound tells the circuit designer that no lossless matching circuit can be found that reduces the VSWR below 6. The plot shows the longer ladders slowly converge to the minimal VSWR. The general ladders allow each stage to be either a series inductor, series capacitor, shunt inductor, or shunt capacitor. The component values constrained to practical values for HF antenna matching: $250 \leq L \leq 12,000$ (nH); $25 \leq C \leq 2,500$ (pF). The State Space line marks the best possible match that can be attained by any lumped, lossless 2-port where the degree d counts the number of reactive elements [2]. For $d = 0$, the matching 2-port is typically a transformer. Figure 3 shows the State Space line plunges past the H^∞ bound and flags that "overfitting" has occured [17].

Overfitting occurs when the finite number of sampled reflectances are overwhelmed by the circuit parameters. This is not a pathological situation—any impedance can be perfectly matched at a single frequency using a series-shunt pair. Given a finite number of frequencies, lossless matching circuits can admit perfect matching at these frequencies. However, the match be-

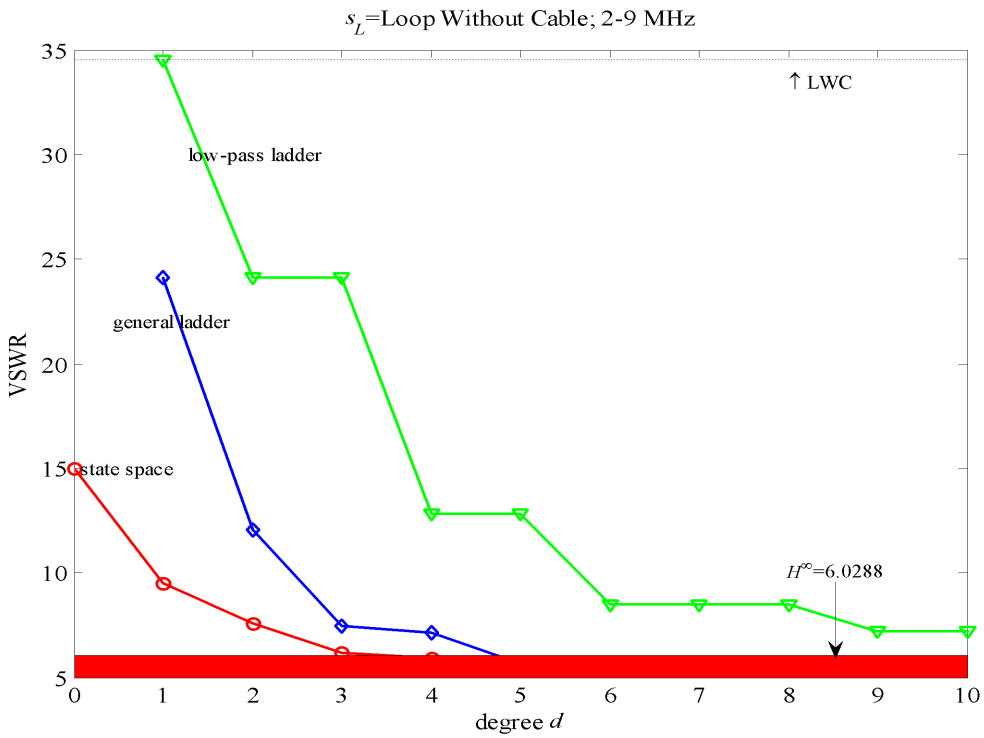

Figure 3: Lossless matching bounds.

tween frequency samples is less than optimal. More formally, whenever a matching family pushes all the sampled reflectances past the H^∞ bound, there will be frequency bands exterior to the sampled frequencies where the match is worse than the H^∞ bound [17].

A similar problem attends the estimate of the H^∞ bound. If the reflectance s_L of the load is sufficiently smooth, the H^∞ bound will be the minimal VSWR attainable by any lumped, lossless 2-port [2]. The numerical estimate of the H^∞ bound presented in the plot is obtained from the sampled reflectance by using splines and extrapolating off the frequency band. Consequently, this numerical H^∞ bound is only an approximation of true H^∞ bound. This approximation can be improved by increasing the sampling density and expanding the frequency band. Figure 3 shows that overfitting is a problem when working with this LWC dataset.

3 Lossless Matching using Ladders

Figure 4 shows the matching results for the LWC using a general ladder of degree 3. The solid curve is the original reflectance. The dotted line is the matched reflectance. The topology of this ladder is reported on the right side of the plot and presented in Figure 5. Because there are three stages with four circuit options per stage, there are $4^3 = 64$ ladders. The index $n_L = 51$ is the optimal's ladder index.

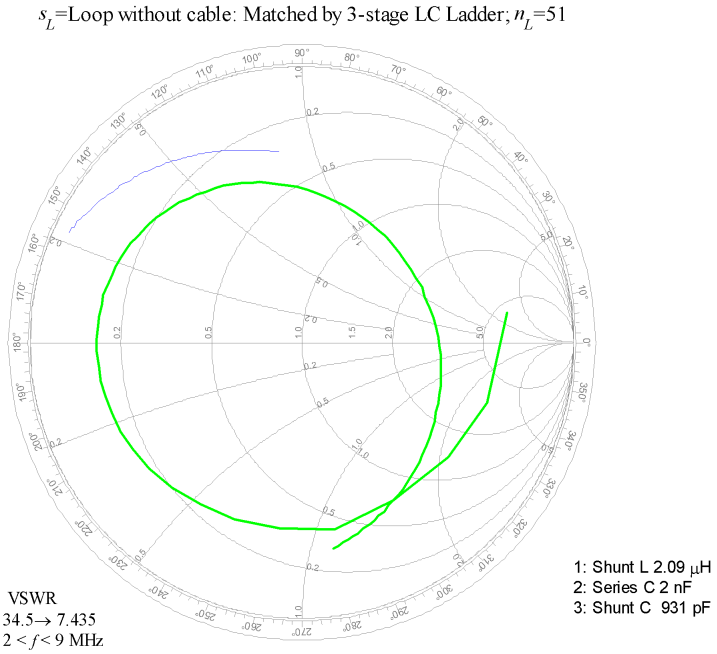

Figure 4: Matching with a general ladder of degree 3.

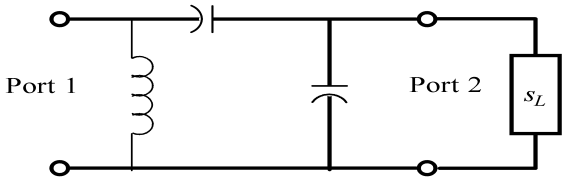

Figure 5: LC ladder $n_L = 51$ for degree 3.

Figures 6 and 7 report the matching and ladder topology for matching the LWC. The solid curve is the reflectance of the LWC and the dotted line is the matched reflectance. The "kinkiness" in the matched reflectance warns that finer sampling is needed.

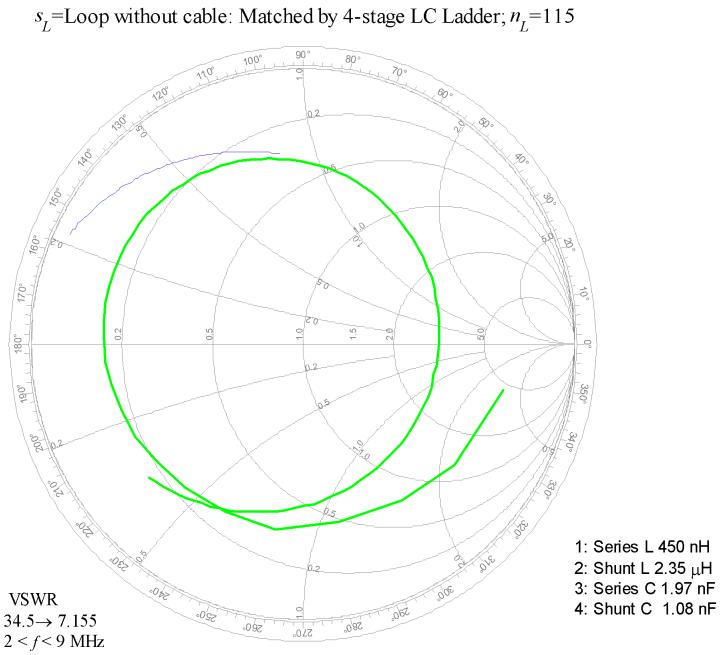

Figure 6: Matching with a general ladder of degree 4.

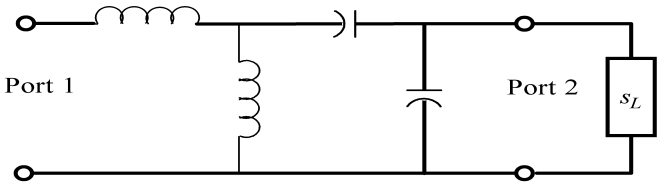

Figure 7: LC ladder $n_L = 115$ for degree 4.

Figures 8 through 13 show the results of matching the LWC with ladders of degree $d = 5$. Although the ladders with degree $d \geq 5$ do overfit, the plots do show the near-circularity of the error curve and the natural extension of the matching circuit topology as a function of the degree.

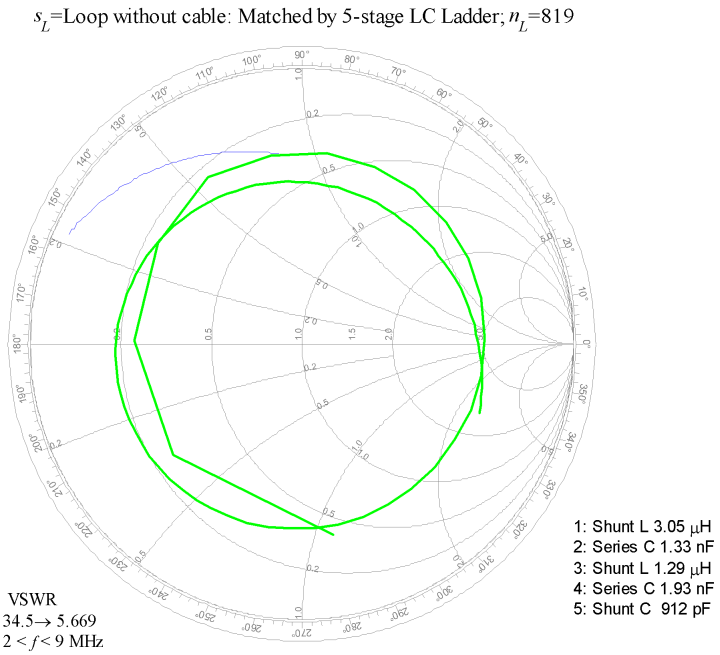

Figure 8: Matching with ladder $n_L = 627$ for degree 5.

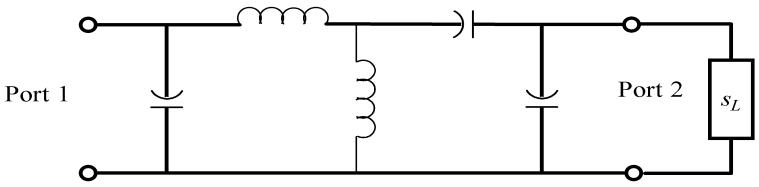

Figure 9: LC ladder $n_L = 627$ for degree 5.

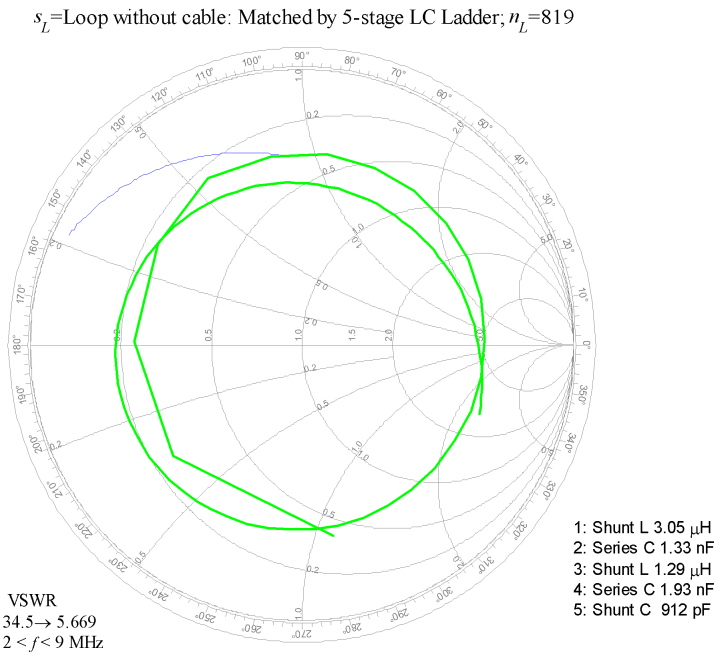

Figure 10: Matching with ladder $n_L = 807$ for degree 5.

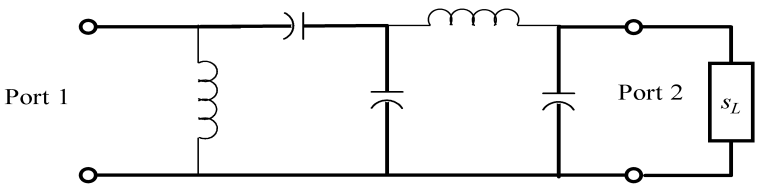

Figure 11: LC ladder $n_L = 807$ for degree 5.

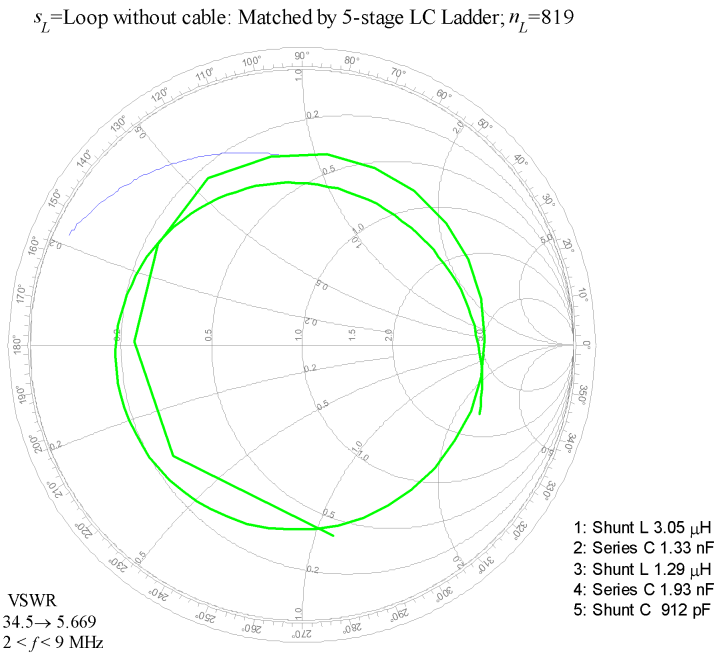

Figure 12: Matching with ladder $n_L = 819$ for degree 5.

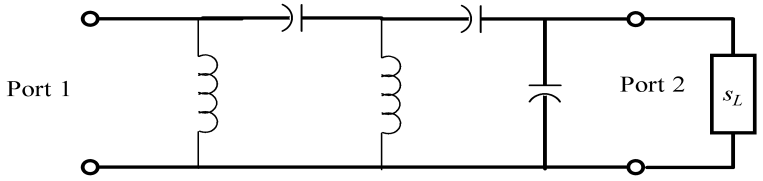

Figure 13: LC ladder $n_L = 819$ for degree 5.

4 Lossy 2-Ports

A review of the power flows in 2-ports is necessary to set up the lossy matching problem. Figure 14 shows the power flows of a 2-port with scattering matrix

$$S = \begin{bmatrix} s_{11} & s_{12} \\ s_{21} & s_{22} \end{bmatrix}$$

connecting a generator to a load. The 2-port is called *lossy*, provided S is a contraction over all frequencies [15, Theorem 4-3]:

$$S(j\omega)^H S(j\omega) \leq \begin{bmatrix} 1 & 0 \\ 0 & 1 \end{bmatrix}.$$

The 2-port is called *lossless*, provided S is unitary over all frequencies:

$$S(j\omega)^H S(j\omega) = \begin{bmatrix} 1 & 0 \\ 0 & 1 \end{bmatrix}.$$

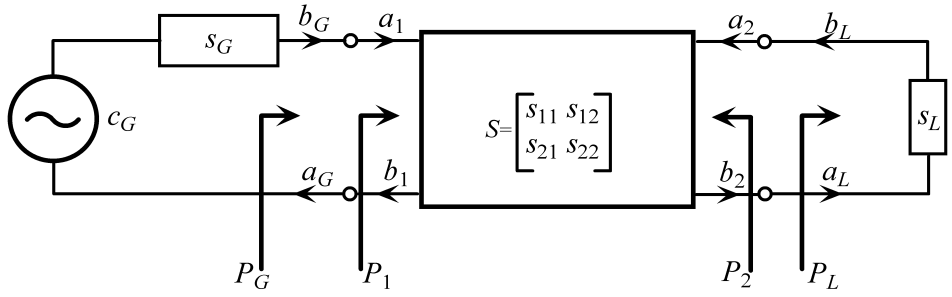

Figure 14: Reflectances and powers.

- The average power delivered to Port 1:

$$P_1 := \frac{1}{2}(|a_1|^2 - |b_1|^2) = \frac{|a_1|^2}{2}(1 - |s_1|^2).$$

- The average power delivered to Port 2:

$$P_2 := \frac{1}{2}(|a_2|^2 - |b_2|^2) = -P_L.$$

- The average power delivered to the load [7, Eq. 2.6.6]:

$$P_L := \frac{1}{2}(|a_L|^2 - |b_L|^2) = \frac{|b_2|^2}{2}(1 - |s_L|^2).$$

- The average power delivered by the generator:

$$P_G = \frac{|c_G|^2}{2}\frac{1 - |s_1|^2}{|1 - s_G s_1|^2}.$$

The reflectance looking into Port 1 is

$$s_1 = s_{11} + s_{12}s_L(1 - s_{22}s_L)^{-1}s_{21} =: \mathcal{F}_1(S, s_L). \tag{1}$$

Similarly, the reflectance looking into Port 2 is

$$s_2 = s_{22} + s_{21}s_G(1 - s_{11}s_G)^{-1}s_{12} =: \mathcal{F}_2(S, s_G). \tag{2}$$

The *maximum power available from a generator* is defined as the average power delivered by the generator to a conjugately matched load [7, Eq. 2.6.7]:

$$P_{G,\max} := P_G|_{s_1 = \overline{s_G}} = \frac{|c_G|^2}{2}(1 - |s_G|^2)^{-1}.$$

The *source mismatch factor* [7, Eq. 2.7.17] is

$$\frac{P_G}{P_{G,\max}} = \frac{(1 - |s_G|^2)(1 - |s_1|^2)}{|1 - s_G s_1|^2}.$$

The *maximum power available from the 2-port* is defined as the average power delivered from the network to a conjugately matched load [7, Eq. 2.6.19]:

$$P_{L,\max} := P_L|_{s_L = \overline{s_2}} := \frac{|b_2|_{s_L = \overline{s_2}}|^2}{2}(1 - |s_2|^2).$$

The *load mismatch factor* [7, Eq. 2.7.25] is

$$\frac{P_L}{P_{L,\max}} = \frac{(1 - |s_L|^2)(1 - |s_2|^2)}{|1 - s_L s_2|^2}.$$

The basic gains are itemized [7, page 213]:

- Transducer power gain:

$$G_T := \frac{P_L}{P_{G,\max}} = \frac{\text{power delivered to the load}}{\text{maximum power available from the generator}}.$$

- Power gain:

$$G_P := \frac{P_L}{P_1} = \frac{\text{power delivered to the load}}{\text{power delivered to the network}}.$$

- Available power gain:

$$G_A := \frac{P_{L,\max}}{P_{G,\max}} = \frac{\text{maximum power available from the network}}{\text{maximum power available from the generator}}.$$

When a general 2-port is used in Figure 14—be it lossless, passive, or active—the transducer power G_T is provided by Pozar [16, Eq. 11.13]:

$$G_T = |s_{21}|^2 \, \frac{(1-|s_G|^2)(1-|s_L|^2)}{|1-s_G s_1|^2 |1-s_{22} s_L|^2}. \tag{3}$$

The transducer power gain is tightly linked to the power mismatches when the 2-port is lossless.

Lemma 1 *[2] If the 2-port of Figure 14 is lossless,*

$$P_1 + P_2 = 0. \tag{4}$$

If the 2-port is lossless and the loads are passive s_G, $s_L < 1$, the transducer power gain has the equivalent forms:

$$G_T = \frac{P_L}{P_{G,\max}} = \frac{P_G}{P_{G,\max}} = \frac{(1-|s_G|^2)(1-|s_1|^2)}{|1-s_G s_1|^2}. \tag{5}$$

Proof: There always holds $P_2 = -P_L$ and $P_G = P_1$. If the 2-port is lossless, the power consumed by the 2-port is zero. Consequently, the power that

flows into the 2-port (P_1) must be equal to the power that flows out of the 2-port ($-P_2$). This proves Equation 4. For the gain,

$$G_T = \frac{P_L}{P_{G,\max}} = \frac{-P_2}{P_{G,\max}} \overset{\text{Eq. 4}}{=} \frac{P_1}{P_{G,\max}} = \frac{P_G}{P_{G,\max}},$$

where the last term is the source mismatch. ///

The proof makes it clear that the equality holds because the power flowing into the lossless 2-port is the power flowing out of the 2-port, which is what one would expect from a lossless 2-port.

The *power mismatch* is the pseudo-hyperbolic distance between $\overline{s}_1$ and s_2 measured along their geodesic [10]:

$$\Delta P(s_1, s_2) := \left| \frac{\overline{s_1} - s_2}{1 - s_1 s_2} \right|. \tag{6}$$

If the 2-port of Figure 14 is lossless, and $s_1,\ s_G < 1$,

$$G_T(s_G, S, s_L) = 1 - \Delta P(s_G, s_1)^2. \tag{7}$$

When $s_G = 0$, Equations 5 and 7 reduce to a handy form:

$$G_T(s_G = 0, S, s_L) = 1 - |s_1|^2. \tag{8}$$

When the 2-port is lossless, we can match at Port 1 or Port 2.

Lemma 2 *[2] If the 2-port of Figure 14 is lossless and $s_1,\ s_G < 1$,*

$$G_T(s_G, S, s_L) = 1 - \Delta P(s_G, \mathcal{F}_1(S, s_L))^2 = 1 - \Delta P(\mathcal{F}_2(S, s_G), s_L)^2.$$

Finally, the VSWR is computed from the input reflectance [16, Eq. 2.41]:

$$\text{VSWR} := \frac{1 + |s_1|}{1 - |s_1|}.$$

The following are equivalent for a *lossless* matching 2-port:

- Maximizing G_T,
- Minimizing the source mismatch,
- Minimizing the load mismatch,
- Minimizing the VWSR.

A lossy 2-port breaks these equivalences. Define the gains at Port 1 and 2 as

$$G_1(s_G, S, s_L) := 1 - \Delta P(s_G, \mathcal{F}_1(S, s_L))^2 = \frac{P_G}{P_{G,\max}},$$

$$G_2(s_G, S, s_L) := 1 - \Delta P(\mathcal{F}_2(S, s_G), s_L)^2 = \frac{P_L}{P_{L,\max}}.$$

Because the lossy 2-port forces G_A, $G_P \leq 1$, the transducer power gain is bounded as follows:

$$G_T = \frac{P_L}{P_{G,\max}} = \frac{P_{L,\max}}{P_{G,\max}} \frac{P_L}{P_{L,\max}} = G_A G_2 \leq G_2$$

$$G_T = \frac{P_L}{P_{G,\max}} = \frac{P_1}{P_{G,\max}} \frac{P_L}{P_1} = G_P G_1 \leq G_1.$$

These bounds break the equivalences—maximizing G_T is not equivalent to minimizing the mismatches or VSWR.

5 Lossy Matching Misconceptions

The bulk of the literature on lossy matching is found in amplifier design problems where gain is traded to reduce noise [14]. For lossy matching to antenna or passive loads, the confusion arises when the VSWR and the transducer power gain are conflated. When matching over the class of **lossless** 2-ports, the following are equivalent:

- Maximizing G_T
- Minimizing VSWR

by Equation 8. However, if the matching 2-ports are lossy, maximizing G_T is **not** equivalent to minimizing the VSWR. Indeed, minimizing the VSWR over the class of lossy 2-ports leads to the bogus solution of Figure 15. A perfect match is achieved by a lossy 2-port—but the antenna does not radiate.[1]

[1] J.C. Allen [2001] Matching Results for the HF-BB Antenna over 2-30 MHz. Report prepared for Lance Koyama, Code D851, Space and Naval Warfare Systems Center, San Diego, CA.

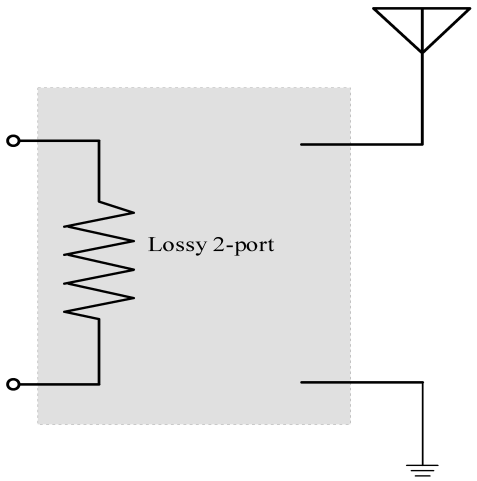

Figure 15: Perfect "matching" by a lossy 2-port.

What are the mathematical results on lossy matching?

The simple inequality

$$\max\{G_T(s_G, S, s_L) : S \text{ lossless}\} \leq \max\{G_T(s_G, S, s_L) : S \text{ lossy}\}$$

follows because the lossless 2-ports are a subset of the lossy 2-ports. However, Ball and Helton [3] showed that the preceeding inequality is actually an equality:

$$\max\{G_T(s_G, S, s_L) : S \text{ lossless}\} = \max\{G_T(s_G, S, s_L) : S \text{ lossy}\}$$

If maximizing transducer power gain is the only objective, the search over all the 2-ports can be restricted to the lossless 2-ports. However, if the antenna designer has multiple objectives, the optimal 2-ports need not be lossless. Consequently, lossy matching will trade transducer power gain to improve another design objective.

6 Multiobjective Lossy Matching

One lossy matching scheme trades transducer power gain against reflected power:

- Maximize the power delivered to the load
- Minimize the reflected power

Because the lossy matching is measured over a frequency band Ω, the maximum or worst reflected power is

$$\|s_1\|_\infty = \max\{|s_1(j\omega)| : \omega \in \Omega\}.$$

The smallest or worst power delivered to the load is

$$\|G_T\|_{-\infty} = \min\{|G_T(j\omega)| : \omega \in \Omega\}.$$

The lossy matching 2-port must simultaneously minimize the largest reflected power while maximizing the smallest transducer power gain:

$$\begin{cases} \text{Maximize } \|G_T\|_{-\infty} \\ \text{Minimize } \|s_1\|_\infty \end{cases}.$$

To formulate as a standard multiobjective problem, all objective functions are minimized:

$$\gamma(\mathbf{x}) = \begin{bmatrix} \gamma_1(\mathbf{x}) \\ \gamma_2(\mathbf{x}) \end{bmatrix} = \begin{bmatrix} 1 - \|G_T(\mathbf{x})\|_{-\infty} \\ \|s_1(\mathbf{x})\|_\infty \end{bmatrix},$$

where the vector $\mathbf{x} \in X$ parameterizes the lossy matching circuit. For example, suppose the lossless matching circuit of degree $d = 3$ is augmented by a series resistor to slide the reflectance into a smaller VSWR. Figure 16 is a diagram of the lossy matching circuit. Let X denote the collection of parameter vectors $\mathbf{x}$ governed by the bounds:

$$\mathbf{x} = \begin{bmatrix} L_1 \\ C_1 \\ C_2 \\ R \end{bmatrix}; \qquad \begin{array}{l} 250 \le L_1 \le 12,000 \text{ (nH)} \\ 25 \le C_1, C_2 \le 2,500 \text{ (pF)} \\ 10^{-6} \le R \le 100 \text{ (ohm)} \end{array}. \tag{9}$$

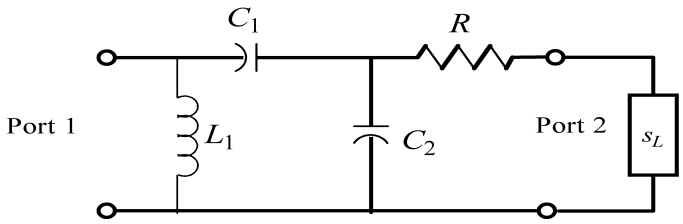

Figure 16: Lossy matching circuit.

The fundamental object is the *performance image*:

$$\gamma(X) := \{\gamma(\mathbf{x}) : \mathbf{x} \in X\}.$$

Minimizing $\gamma : X \to \mathbb{R}$ is the search for all the *minimal elements* of $\gamma(X)$. Any $\gamma(\mathbf{x})$ is a minimal element [5, page 21] of $\gamma(X)$, provided

$$\gamma(\mathbf{y}) \leq \gamma(\mathbf{x}) \implies \gamma(\mathbf{y}) = \gamma(\mathbf{x}).$$

If $\gamma(\mathbf{x})$ is a minimal element of $\gamma(X)$, its preimage $\mathbf{x} \in X$ is called *Pareto optimal* [5, page 102]. Figure 17 illustrates the minimal elements of $\gamma(X)$ as the dark line on the boundary of $\gamma(X)$. The dark line is also the image of the Pareto optima and is called the *Pareto front* [13].

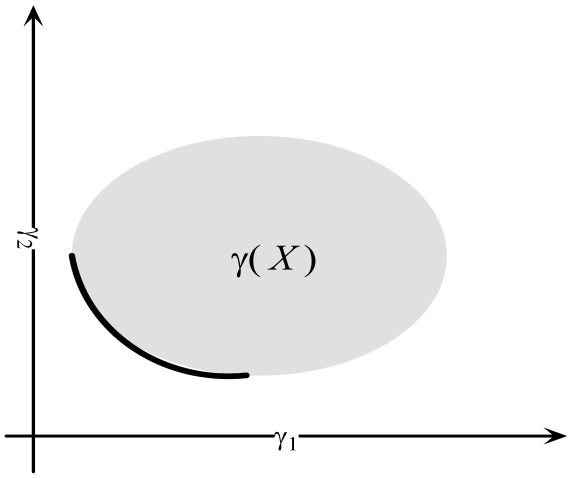

Figure 17: The Pareto front.

Das and Dennis [6] emphasize,

> *The fundamental goal of Multiobjective Optimization is the computation of all Pareto optima.*

However, from a circuit designer's view, it is the Pareto front that reveals the design tradeoffs. Figure 18 plots the (estimated) Pareto front of the lossy 2-port of Figure 16. For context, the performance image $\gamma(X)$ is also estimated. The blue dots that fill out the performance image $\gamma(X)$ are random samples of the parameter vectors $\mathbf{x} \in X$.

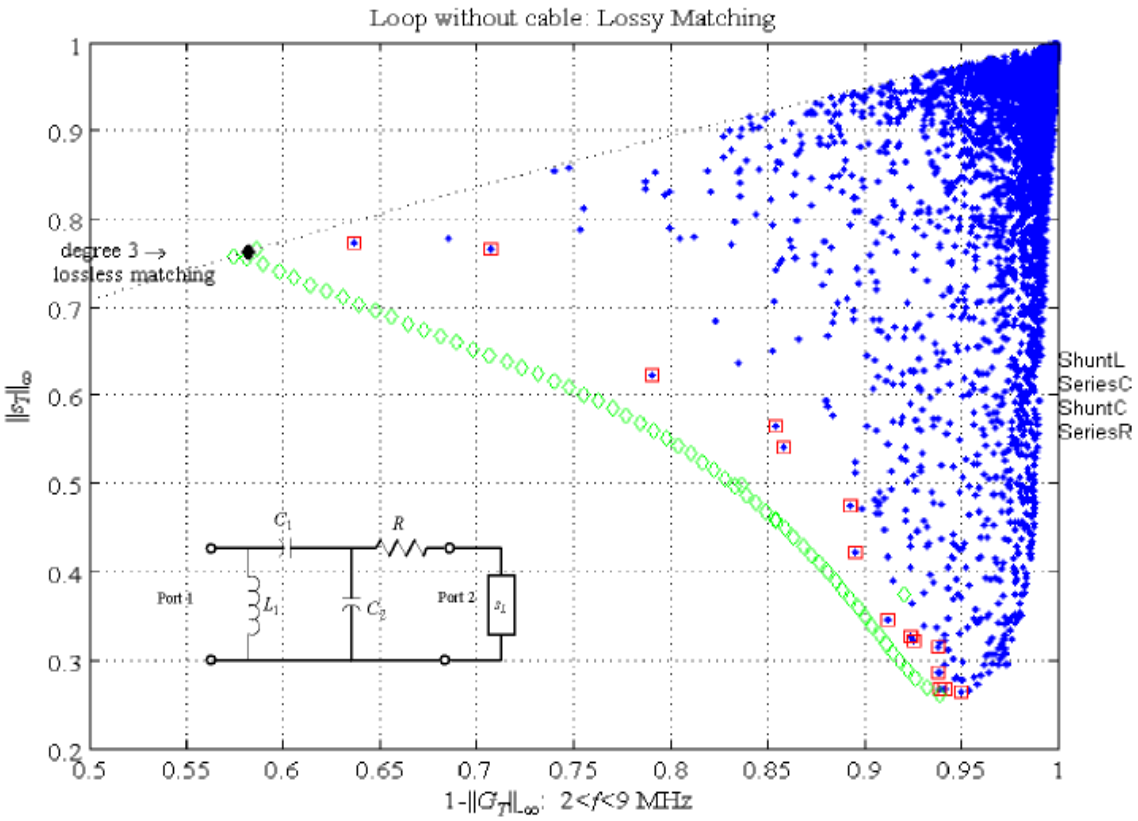

Figure 18: Performance image of the lossy matching circuit.

Basic to understanding the performance image $\gamma(X)$ is the lossless performance curve marked by the dotted black line. If the 2-port is lossless, Equation 8 forces the square-root relation

$$\|s_1\|_\infty = \sqrt{1 - \|G_T\|_{-\infty}}. \tag{10}$$

Equation 10 is the dotted black line in Figure 18 and shows that the lossless circuits form part of the boundary of $\gamma(X)$. The black diamond on the lossless performance curve marks performance of the ladder of Figure 3. The red boxes are the images of the Pareto points relative to the random samples. Equivalently, the red boxes are the minimal elements of the set of blue dots. The pre-images of these red boxes are the starting points of the multiobjective minimizer. The green diamonds are the terminating points of the multiobjective minimizer. The plot does show that the minimizer can be trapped in a local minimum. The green diamonds approximate the Pareto front to show the best tradeoff between transducer power gain and reflectance. For example, if the circuit design must have a VSWR not exceeding 4, which corresponds to $\|s_1\|_\infty = 0.6$, the Pareto front shows that the transducer power gain is limited to

$$\|G_T\|_{-\infty} = -6.1 \quad \text{[dB]}.$$

Section 9 compares various Pareto fronts using an engineer's point-of-view where the tradeoff is made between VSWR and insertion loss.

Figure 19 presents the estimated Pareto points or the pre-image of the green diamonds. The domain of γ consists of four variables: the two capacitors, the inductor, and the resistor. The two plots show the joint variation of the estimated Pareto points. Traveling on the Pareto front starting from the lossless point ($R = 0$) corresponds to traveling on the inductor-resistor curve starting from the bottom of the plot and the capacitor curve from the top of its plot. This plot illustrates two points. First, the domain of γ is really not amiable to visualization—the number of variables quickly exceeds credible plotting techniques. Second, although the values of the matching circuit necessary to engineer a particular circuit, the domain of γ simply does not reveal the tradeoffs. Consequently, computation of the performance image and Pareto front is more valuable to the circuit designer.

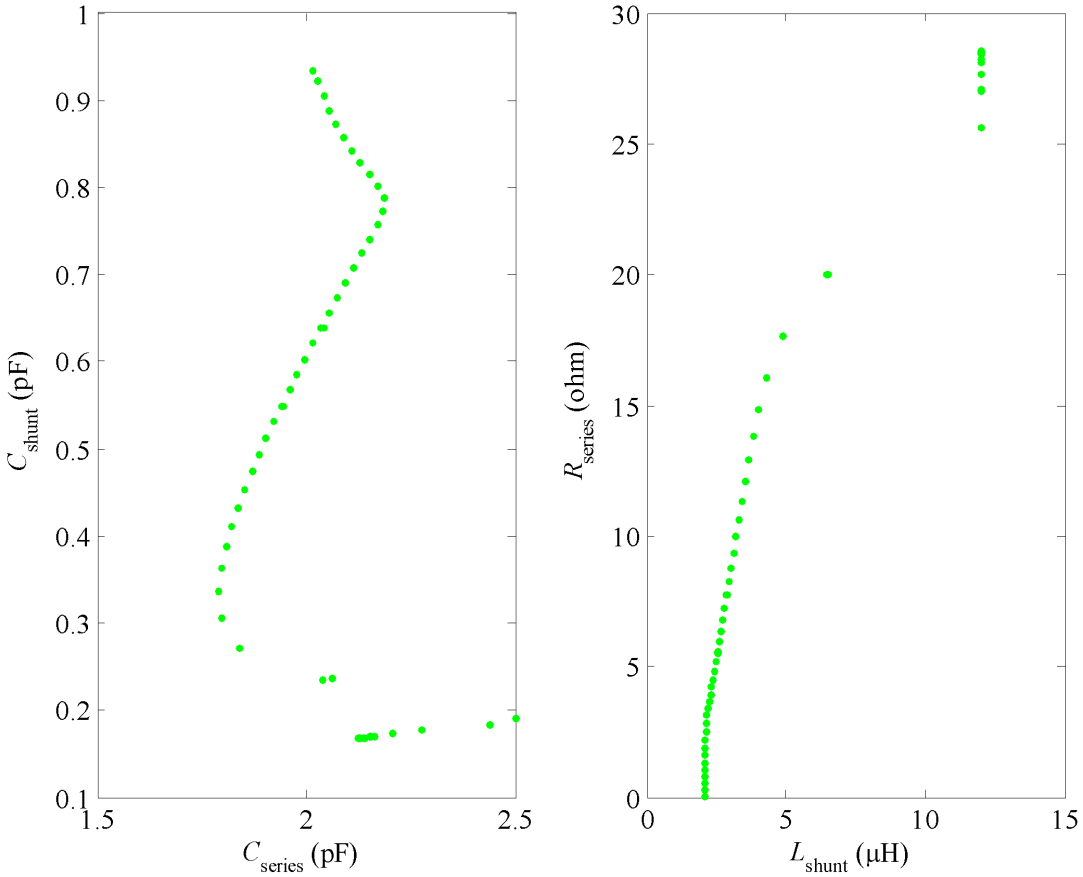

Figure 19: Pareto points.

If visualizing the performance image is the goal, *Why not simply fill out the performance image $\gamma(X)$ with random points?* Dense sampling simply requires a fast computer and avoids running a multiobjective minimizer. Unfortunately, a dense filling of performance image $\gamma(X)$ for this degree 3 ladder requires at least 10 million points. Higher order ladders require even more points. Consequently, coarse sampling coupled with a minimizer is a more feasible approach to compute this Pareto front. Figures 20 and 21 assess this approach using the degree 5 ladder of Figure 9. Instead of the 5,000 samples used in the preceding degree 3 ladder, Figure 20 uses only 1,000 random samples.

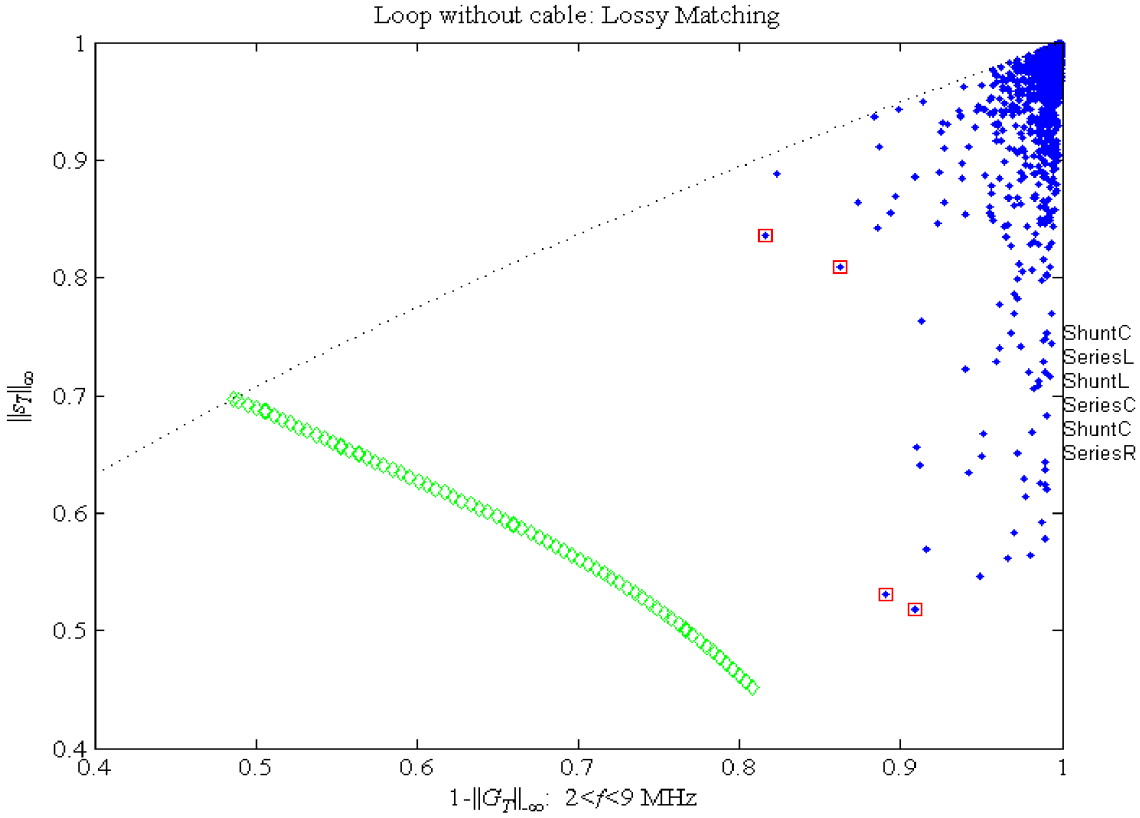

Figure 20: Gain-Reflectance for degree 5 ladder.

Although the Pareto front has better gain and smaller VSWR than the Pareto front of the degree 3 ladders, two observations are in order. First, not all of the Pareto front was obtained. Figure 21 shows the result of running the same simulation with 100,000 random samples to fill out the performance image. Even so, the lower tail of the performance image is still missing. Consequently, extreme sampling is necessary to get good starting points for the minimizer. The second observation is that the H^∞ computations in Figure 3 warn that these ladders are likely overfitting the data—the improved performance is likely an artifact of insufficient sampling. Additional insight can be obtained by considering the orbits of the resistors.

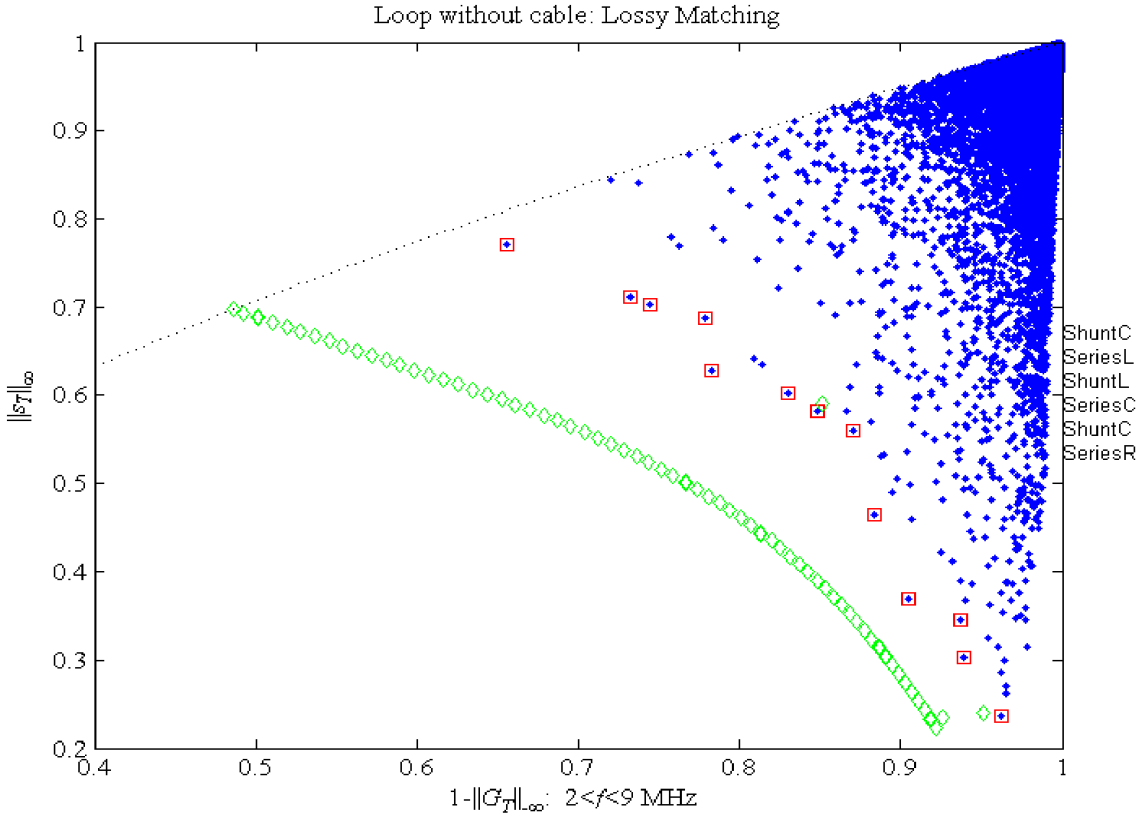

Figure 21: Increased sampling for degree 5 ladder.

7 Orbits of the Resistor

The notion of an orbit is a basic concept in circuit synthesis and matching [8], [10], [4]. Let $\mathcal{S}$ denote a collection of matching 2-ports. Each element $S \in \mathcal{S}$ acts on the load s_L as

$$s_1 = \mathcal{F}_1(S, s_L) = s_{11} + s_{12}s_L(1 - s_{22}s_L)^{-1}s_{21}.$$

The collection of all these reflectances denoted

$$\mathcal{F}_1(\mathcal{S}, s_L) := \{\mathcal{F}_1(S, s_L) : S \in \mathcal{S}\}$$

and called is the *orbit of s_L under the action of $\mathcal{S}$*. The orbit contains all reflectances that are available to the circuit designer using the action of the 2-ports in $\mathcal{S}$.

Basic to lossy matching is controlling the number and size of the resistors. A series resistor is common to all the preceding matching designs because a series resistor moves the LWC antenna toward optimal match. If the 2-port is a series resistor, the orbit of the LWC antenna is

$$\left\{ \frac{z_L + R/Z_0 - 1}{z_L + R/Z_0 + 1} : R > 0 \right\}$$

and illustrated in Figure 22.

From a circuit designer's view, the images of the orbits are the useful design objects. Figure 23 plots the images of the orbits through each of the minimal elements. If a minimal element has performance $\gamma(\mathbf{x})$ where

$$\mathbf{x} = \begin{bmatrix} L_1 \\ C_1 \\ C_2 \\ R_0 \end{bmatrix},$$

the image of the orbit through the minimal element is

$$\{\gamma(\mathbf{x}(R)) : R \geq 0\}; \quad \mathbf{x}(R) := \begin{bmatrix} L_1 \\ C_1 \\ C_2 \\ R \end{bmatrix}.$$

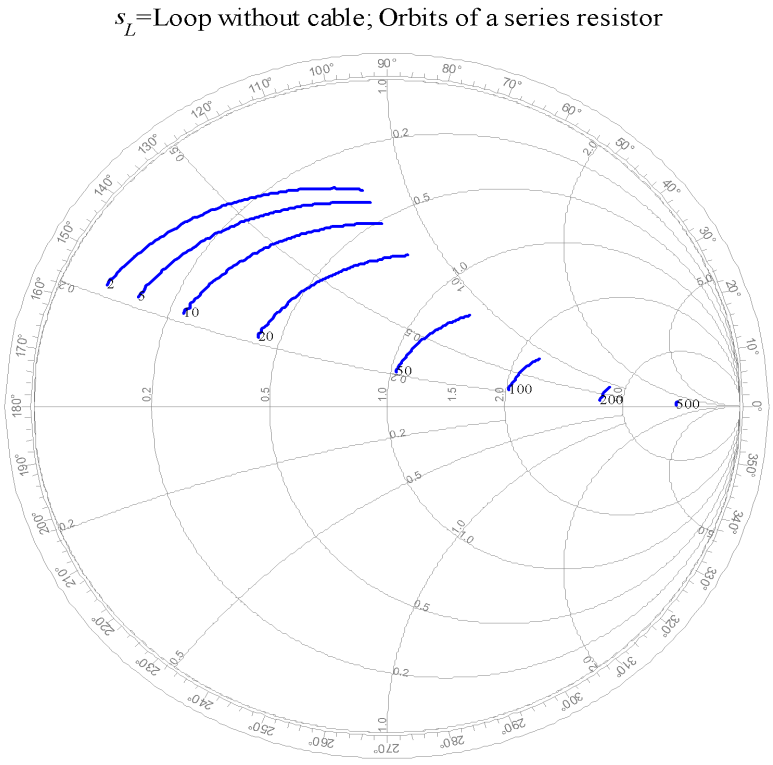

Figure 22: Action of a series resistor.

When $R = 0$, the matching circuit is lossless and this lossless end of the orbit lands on the lossless curve of Equation 10. When the resistor gets large, the orbits all fold into the "distopic point"

$$\gamma = \begin{bmatrix} 1 \\ 1 \end{bmatrix}$$

that corresponds to the biggest possible reflection and the smallest possible gain. Figure 23 shows that a handful of orbits can fill out the performance image $\gamma(X)$ and map out the Pareto front. This technique requires dense sampling to get minimal elements that have interesting orbits. Here, "interesting" means that these orbits fill up the performance image to reveal the Pareto front.

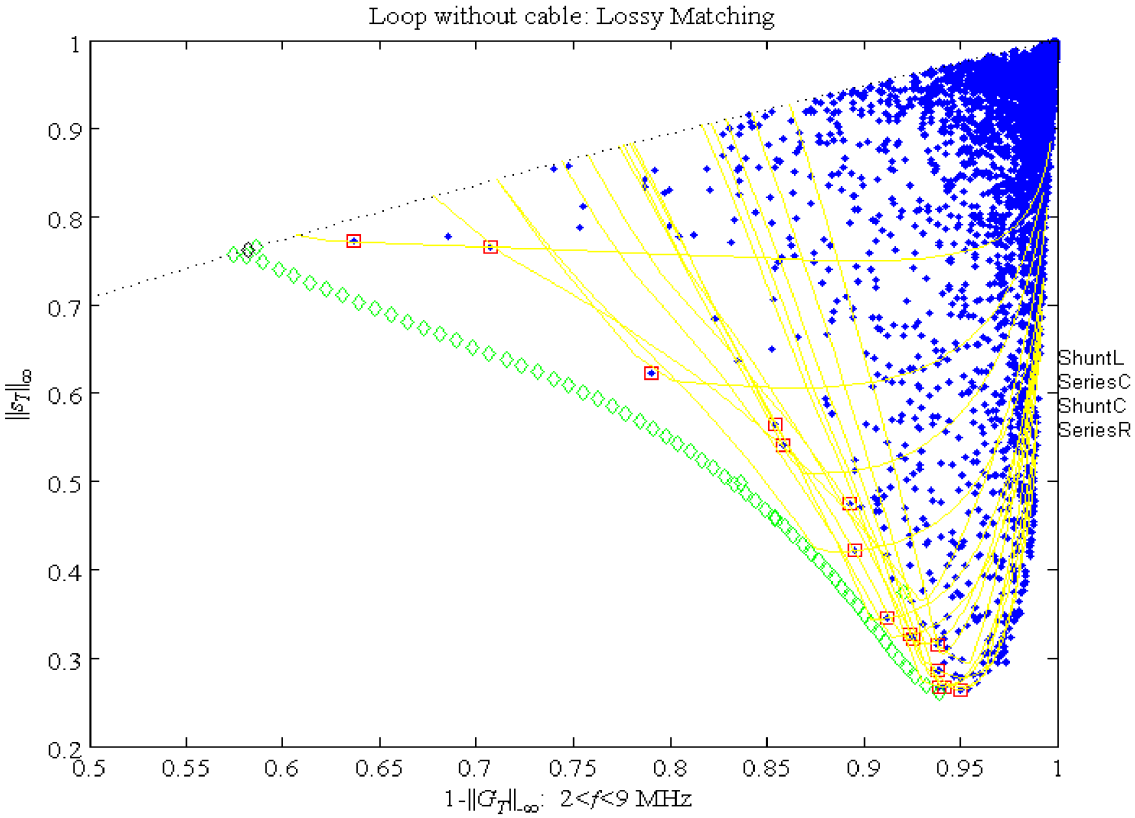

Figure 23: Orbits of the series resistor through the minimal elements ($d = 3$).

Another algorithm to compute the Pareto front—also without restoring to extreme sampling—simply lumps the lossy part into the given load. For example, fix a resistor value. Minimize the reflectance over the *lossless* part of the matching circuit. When the resistor is included, the resulting *lossy* matching circuit is close to optimal and is also an excellent starting point of the multiobjective minimizer.

Figure 24 applies this algorithm to the ladders of degree 3. The resulting points are plotted in magenta. and are a good approximation to the Pareto Front (green diamonds). For reference, the random sampling of the performance image are shown as the blue dots. As before, the resulting minimal elements are marked with the red boxes. In more detail, the lossless part of

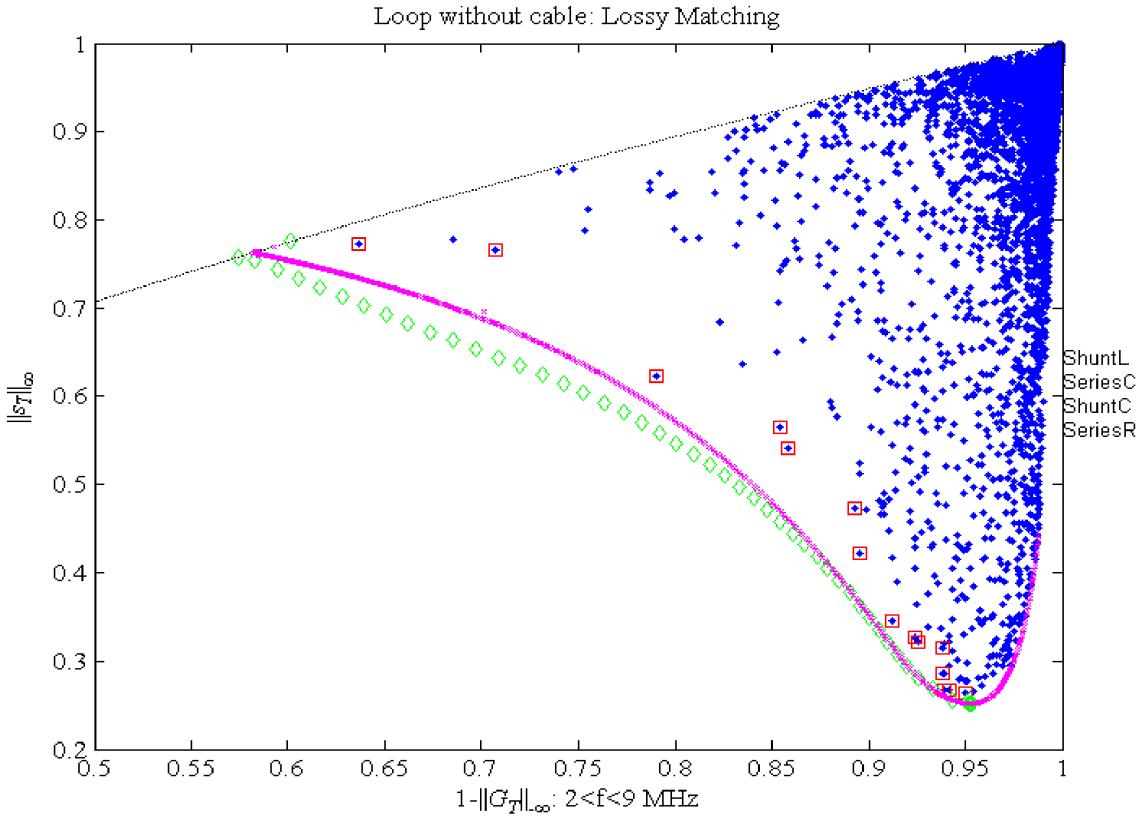

Figure 24: Pareto front approximation by lossless matching ($d = 3$).

the ladders are parameterized as

$$\mathbf{x} := \begin{bmatrix} L_1 \\ C_1 \\ C_2 \end{bmatrix} \qquad \begin{array}{l} 250 \le L_1 \le 12,000 \quad \text{(nH)} \\ 25 \le C_1, C_2 \le 2,500 \quad \text{(pF)} \end{array} .$$

Let X denote the collection of these $\mathbf{x}$'s. For each fixed resistor value R, a lossless matching 2-port was calculated by running the single-objective problem on the VSWR or reflectance:

$$\mathbf{x}_R = \operatorname{argmin} \left\{ \gamma_2 \left(\begin{bmatrix} \mathbf{x} \\ R \end{bmatrix} \right) : \mathbf{x} \in X \right\} .$$

The resulting magenta curve

$$R \mapsto \gamma\left(\begin{bmatrix} \mathbf{x}_R \\ R \end{bmatrix}\right) \quad (10^{-6} < R < 10^2)$$

is a good approximation to the Pareto front.

This algorithm has several benefits. First, fast techniques for solving the lossless problem leverage into this lossy approach. Second, if the intermediate steps of each minimization are plotted in the performance image, a better "filling in" of the image is produced because many of the intermediate points will be close to the Pareto front. Finally, this algorithm can encompass any successful lossless matching scheme—including the H^∞ minimizers.

8 H^∞ Orbits of the Resistor

The H^∞ techniques compute the smallest possible power mismatch attainable over all lossless 2-ports [10], [17], [2]. The H^∞ techniques can be adapted to the lossy matching problem to compute the best possible Pareto front by sweeping over the orbits of the resistor. Figure 25 shows the setup and the power flows. The idea is to sweep over all lossless 2-ports while holding the resistor at a fixed value. The corresponding optimal point in the Gain-Reflectance plane is computed using the H^∞ techniques. The resulting collection of optimal points will contain the best possible Pareto front attainable by any matching circuit consisting of a lossless 2-port chained to a series resistor.

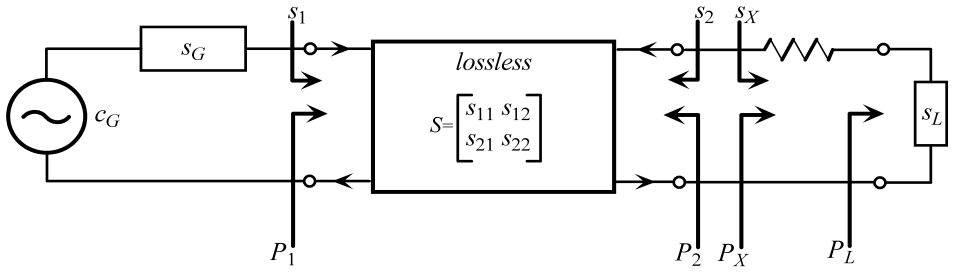

Figure 25: Lossy matching power flows.

For a fixed resistor, the multiobjective function $\gamma(S)$ is parameterized by the scattering matrix of the lossless 2-port S of Figure 25:

$$S = \begin{bmatrix} s_{11} & s_{12} \\ s_{21} & s_{22} \end{bmatrix} \mapsto \begin{bmatrix} 1 - \|G_T(S)\|_{-\infty} \\ \|s_1(S)\|_\infty \end{bmatrix} = \begin{bmatrix} \gamma_1(S) \\ \gamma_2(S) \end{bmatrix} = \gamma(S).$$

The reflectance s_1 is given by Equation 1:

$$s_1(S) = \mathcal{F}_1(S, s_X) = s_{11} + s_{12}s_X(1 - s_{22}s_X)^{-1}s_{21},$$

where s_X is the reflectance looking into the resistor in series with the load s_L. Let Z_0 denote the normalizing impedance. If Z_L denotes the impedance of the load,

$$s_L = \frac{Z_L - Z_0}{Z_L + Z_0} = \frac{z_L - 1}{z_L + 1},$$

where $z_L = Z_L/Z_0$ is the normalized impedance of the load. If R is the value of the resistor,

$$s_X = \frac{Z_L + R - Z_0}{Z_L + R + Z_0} = \frac{z_L + r - 1}{z_L + r + 1},$$

where $r = R/Z_0$ is the normalized resistor value.

Each scattering matrix S is a 2×2 matrix-valued function analytic on the right-half plane $\mathbb{C}_+$ that takes unitary values on the frequency axis. If $U^+(2)$ denotes the set of the scattering matrices of all lossless 2-ports [10]:

$$U^+(2) = \left\{ S \in H^\infty(\mathbb{C}_+, \mathbb{C}^{2\times 2}) : S^H(j\omega)S(j\omega) = \begin{bmatrix} 1 & 0 \\ 0 & 1 \end{bmatrix} \right\},$$

the multiobjective problem for a *fixed* resistor is formalized as

$$\min\{\gamma(S) : S \in U^+(2)\}.$$

Although a theory of multiobjective H^∞ optimization [12] exists, practical implementations are not yet available. However, single-objective H^∞ minimization can compute upper and lower bounds of a minimal element $\gamma(U^+(2))$. Plotting these bounds as a function of the resistor value produces two curves in the Gain-Reflectance plane that contain the best possible Pareto front.

Referring to Figure 25, introduce the transducer power gain G_X defined with respect to the lossless 2-port terminated in load s_X:

$$G_X = \frac{P_X}{P_{G,\max}}.$$

Lemma 2 forces

$$G_X = 1 - \Delta P_1^2 = 1 - \Delta P_2^2.$$

If the minimal power mismatches are denoted as

$$\Delta P_{1,U^+} := \inf\{\|\Delta P(s_G, \mathcal{F}_1(S, s_X))\|_\infty : S \in U^+(2)\}$$

$$\Delta P_{2,U^+} := \inf\{\|\Delta P(\mathcal{F}_2(S, s_G), s_X)\|_\infty : S \in U^+(2)\},$$

Lemma 2 computes the best possible gain as

$$G_{X,U^+} := 1 - \Delta P_{2,U^+}^2 = 1 - \Delta P_{1,U^+}^2.$$

If the generator's reflectance is zero $s_G = 0$,

$$\begin{aligned} \Delta P_{2,U^+} &= \inf\{\|\Delta P(\mathcal{F}_2(S, s_G), s_X)\|_\infty : S \in U^+(2)\} \\ &= \inf\{\|\Delta P(s_2, s_X)\|_\infty : s_2 \in BH^\infty\}, \end{aligned} \tag{11}$$

where last equality is obtained by Darlington's Theorem [2]. The H^∞ techniques of Helton [10] compute the last infimum. This computation produces the smallest reflectance $\|s_1\|_\infty$ looking into Port 1:

$$\gamma_{r,2} = \inf\{\|s_1(S)\|_\infty : S \in U^+(2)\} = \Delta P_{2,U^+}. \tag{12}$$

Let $S_k \in U^+(2)$ be a minimizing sequence:

$$\gamma_{r,2} = \lim_{k\to\infty} \|s_1(S_k)\|_\infty.$$

Any cluster point of the set $\{\gamma(S_k)\}$ is a minimal element of the closure of $\gamma(U^+(2))$. Let γ_r denote a cluster point. The first component $\gamma_{r,1}$ will be bounded using gain estimates obtained from the H^∞ methods.

The biggest possible transducer power gain that can be delivered to the load in series with the resistor is

$$G_{X,U^+} := \sup\{\|G_T(S)\|_{-\infty} : S \in U^+(2)\} = 1 - \Delta P_{2,U^+}^2.$$

However, the first component of $\gamma(S)$ is the transducer power gain

$$G_T = \frac{P_L}{P_{G,\max}}.$$

This transducer gain factors as

$$G_T = \frac{P_X}{P_{G,\max}} \ \frac{P_L}{P_X} = G_X \ G_P,$$

where G_P is the power gain of the 2-port consisting of the series resistor terminated in the load s_L. The G_P factor is computable. The series resistor has a chain matrix

$$T_r = \begin{bmatrix} 1 & R \\ 0 & 1 \end{bmatrix}.$$

This chain matrix maps to its scattering matrix S_r [16, Table 4.2] as

$$T_r \mapsto S_r = \frac{1}{r+2} \begin{bmatrix} r & 2 \\ 2 & r \end{bmatrix} = \begin{bmatrix} s_{r,11} & s_{r,12} \\ s_{r,21} & s_{r,22} \end{bmatrix}.$$

The power gain G_P [16, Eq. 11.8] is

$$G_P = \frac{|s_{r,21}|^2}{1-|s_X|^2} \ \frac{1-|s_L|^2}{|1-s_{r,22}s_L|^2}.$$

Consequently, the best possible transducer power gain is also computable by the H^∞ minimization of Equation 11. Because G_P does not depend on the lossless 2-port, the inequalities

$$\|G_X(S)\|_{-\infty}\|G_P\|_{-\infty} \le \|G_T(S)\|_{-\infty} \le \|G_X(S)\|_{-\infty}\|G_P\|_{\infty}$$

bound the maximum transducer power gain over $U^+(2)$ as

$$G_{X,U^+}\|G_P\|_{-\infty} \le G_{T,U^+} \le G_{X,U^+}\|G_P\|_{\infty}. \tag{13}$$

Equation 12 and 13 show that

$$\begin{bmatrix} 1-G_{X,U^+}\|G_P\|_{\infty} \\ \Delta P_{2,U^+} \end{bmatrix} \le \begin{bmatrix} \gamma_{r,1} \\ \gamma_{r,2} \end{bmatrix} \le \begin{bmatrix} 1-G_{X,U^+}\|G_P\|_{-\infty} \\ \Delta P_{2,U^+} \end{bmatrix}.$$

Figure 26 illustrates these H^∞ bounds. As the series resistor sweeps from 0 to 100 ohms, the corresponding minimal reflectances and gain bounds are plotted. The upper bound makes an excellent design challenge while the lower bound is too coarse for practical use.

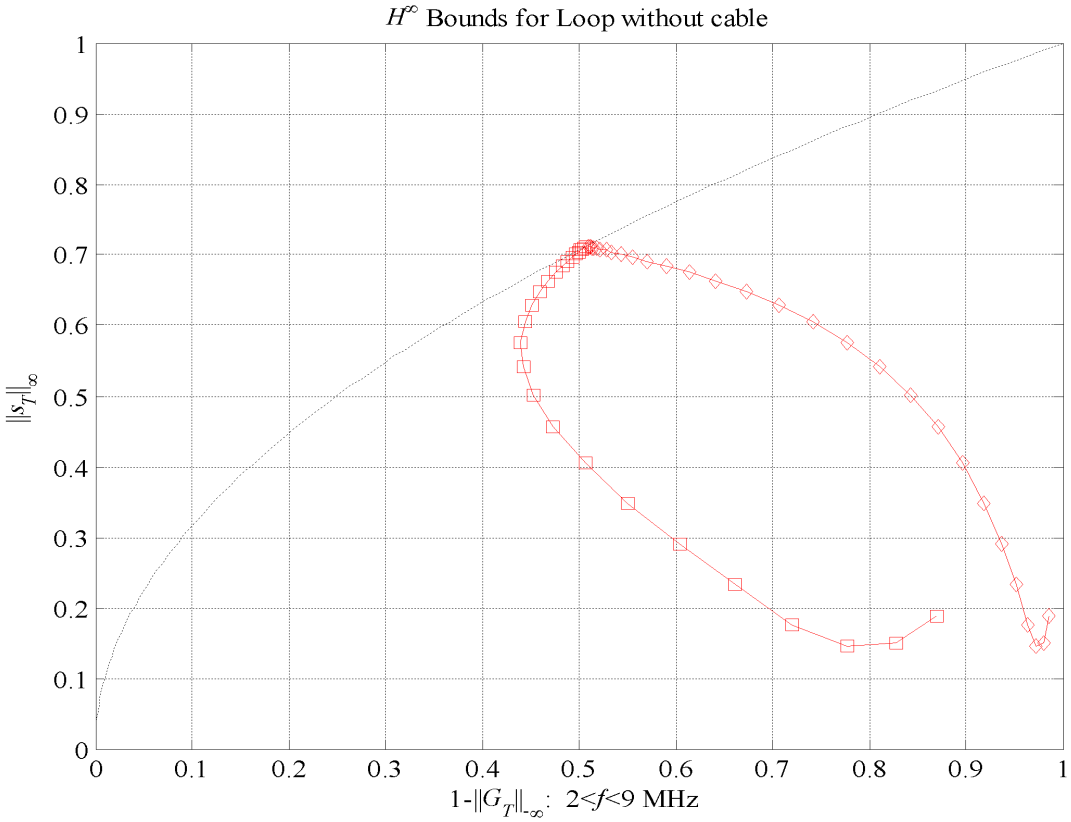

Figure 26: H^∞ bounds.

9 Lossy Matching Design Curves

The preceding plots were graphed in the context of multiobjective minimization—all objectives are minimized and plotted on a linear scale. Consequently, glancing at such a plot to see the tradeoffs in an engineering context is difficult. This section presents the design curves and tradeoffs in a graphical language amiable to the RF engineer.

The Pareto front is a design curve that reveals the tradeoff between minimizing the reflection coefficient and maximizing the transducer power gain. By plotting the reflection coefficient as the VSWR and the gain as transmission loss, design tradeoffs can be readily visualized by an RF engineer. The

reflection coefficient maps to the VSWR as

$$\text{VSWR} = \frac{1 + \|s_1\|_\infty}{1 - \|s_1\|_\infty}.$$

The transducer power maps to the transmission loss as

$$\text{TL} = -10 \log_{10}(\|G_T\|_{-\infty}).$$

Figure 27 compares two Pareto fronts in this TL-VSWR performance plane. The green diamonds mark the Pareto front for the ladder of degree 4 (from Figure 18). The magenta plus signs mark the Pareto Front for the ladder of degree 5 from Figure 21. The black line plots relationship of between VSWR and transmission loss for lossless matching (Equation 10).

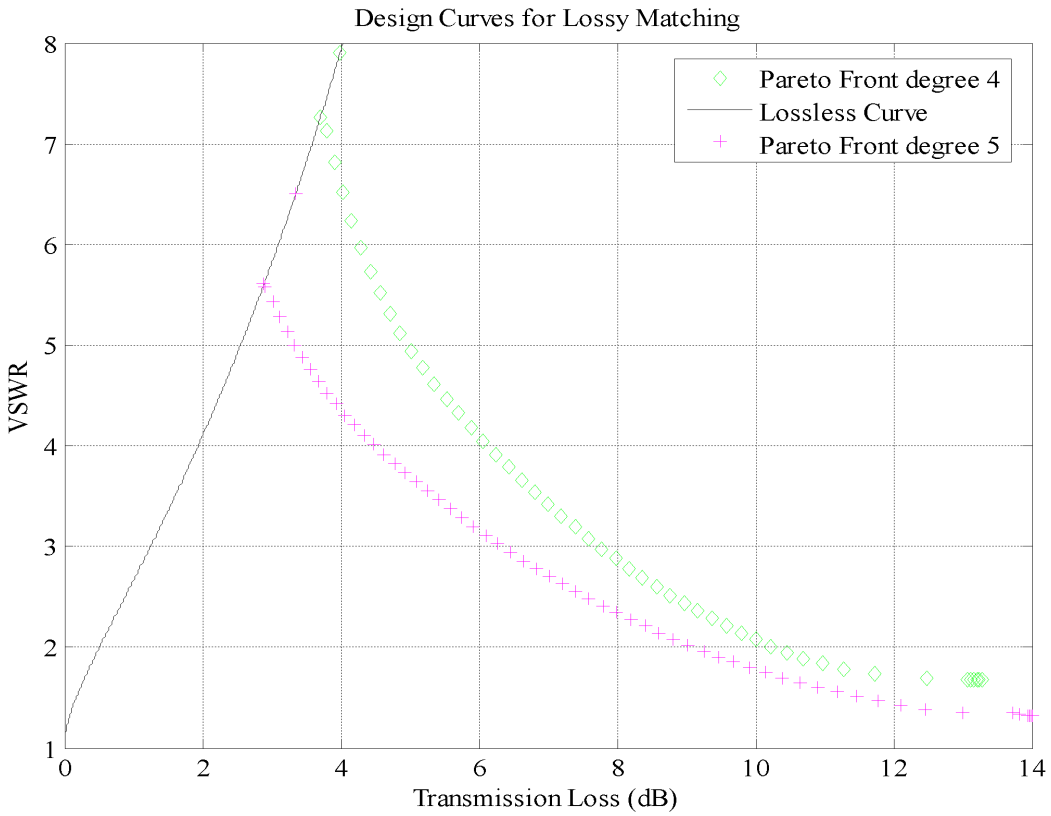

Figure 27: Design objectives from the engineer point-of-view.

By using the design curves, the tradeoff between lowering the VSWR and the transmission loss is easily read. For the network of ladder of degree 4, reducing the VSWR from 7.155 to 4 forces approximately about 2.5 dB of gain to be lost in the resistor. Similarly, for the ladder of degree 5, reducing the VSWR from 5.713 to 4 costs approximately 1.5 dB of gain. Depending on the VSWR requirement, the gain lost to the resistor might be substantial. The engineering tradeoff can be quickly analyzed without having to actually design a matching circuit. If the transmission loss is more than can be accommodated for a given VSWR, the antenna may have to be redesigned to better meet the requirements.

10 Lossy Matching Designs

This lossy matching problem offers splendid research and design opportunities at the interface of mathematics and electrical engineering. Ball and Helton's [4] deep mathematics show that maximizing the transducer power gain over the *lossy* 2-ports is equivalent to matching over the smaller set of *lossless* 2-ports. Attempts to evade the mathematics lead to the bogus designs of Section 5. An engineer would interpret the mathematics with the observation that gain is not improved by wasting power to heat a resistor. Therefore, lossy matching only makes sense when gain is traded to improve another objective. Consequently, lossy matching immediately forces the multiobjective approach of Section 6.

Section 6 shows that the engineer needs the entire Pareto front to visualize the best possible tradeoffs between the competing objectives. This section also showed that, even for a small problem, brute-force sampling simply cannot "fill in" the performance image $\gamma(X)$. Without a sampling near the entire Pareto front, complete computation of the entire Pareto front is impossible. To overcome this computational impasse, the orbit technique was introduced in Section 7 to rapidly "fill in" the performance image $\gamma(X)$ while Section 8 developed H^∞ bounds that map out a region containing the performance image.

Figure 28 illustrates these results by plotting the Pareto fronts for selected ladders and the H^∞ bounds. The H^∞ bounds are not tight—the bounds only delineate a region that contains the best possible Pareto front. The goal of

the designer is to get a matching circuit's Pareto front into that region. The degree 3 ladder tracks the upper bound while the degree 5 ladder is in the region. The degree 5 ladder also breaks the best possible lossless bound located on the square-root relation of Equation 8. Section 2 pointed out that the degree 5 ladders are overfitting in the lossless case. Consequently, the improved performance of the degree 5 ladder is an artifact of overfitting. As such, the degree 3 ladder's Pareto front is the optimal design curve for lossy matching.

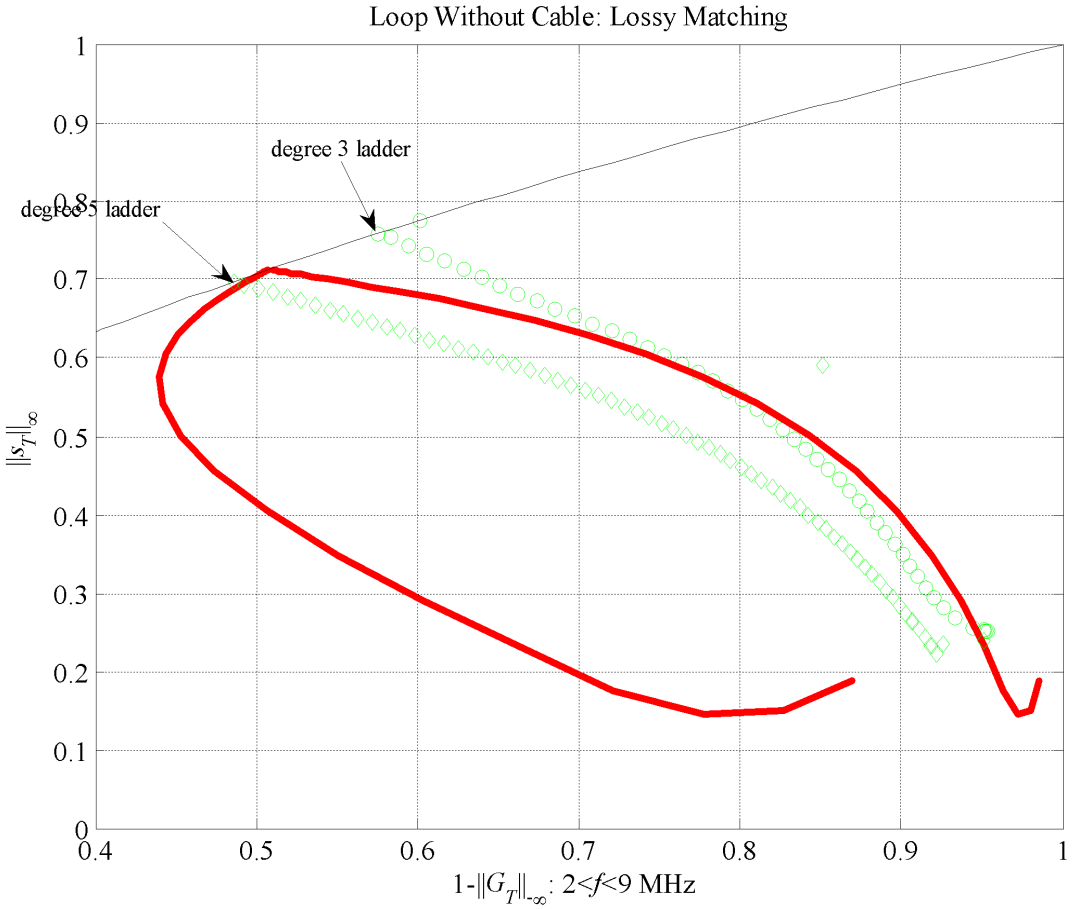

Figure 28: Pareto fronts of the ladders and the upper and lower H^∞ bounds.

Generalizing the orbit technique and comparing other Pareto front computations such as the NBI method is an excellent research topic. Likewise, the H^∞ approach needs improvement to the best possible bounds. Accordingly, two mathematical problems distill from the lossy matching problem:

- Assess the orbit technique for fast Pareto front computation [6].
- Develop computational methods for multiobjective H^∞ bounds [12].

The Pareto front offers a straightforward visualization of the tradeoffs available from an entire family of lossy matching circuits. However, the lossy part of the matching circuit was restricted to a resistor placed in series with the load. Exploring alternative circuits is a classic engineering research task:

- Find better lossy matching circuits.

Such explorations are undertaken in the appendices based the H^∞ bounds [2]. If a lossless 2-port attains the best possible match, the input reflectance is a circle in the Smith chart. Given a circular reflectance, only a slight amount of attenuation will be needed to further pull the circle towards the origin. Consequently, lossy matching should consist of a lossless and reactive circuit connected to the load and its input port connected to a non-reactive attenuator as shown in Figure 29. The results in the appendices support this assertion.

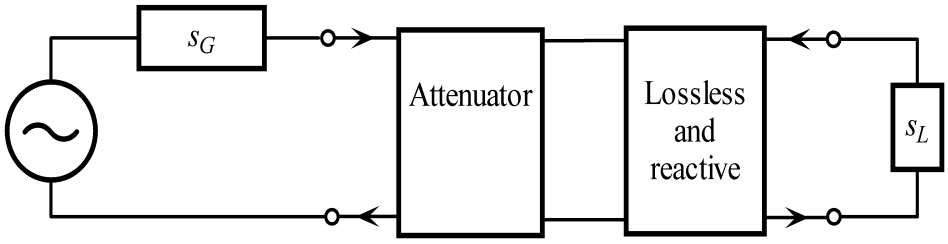

Figure 29: Is this a canonical lossy matching circuit?

References

[1] Allen, J. C. and D. F. Schwartz [2001] Optimal Impedance Matching by Lossless 2-Ports of Specified Degree Independent of Circuit Topology, *Applied Computational Electromagnetics*, 17th Annual Conference Proceedings, pages 588-593.

[2] Allen, J. C. and Dennis Healy [2003] Nehari's Theorem and Electric Circuits, and Analog Signal Processing in *Modern Signal Processing*, Edited by Daniel Rockmore and Dennis Healy, Springer-Verlag, New York, NY.

[3] Ball, Joseph A. and J. William Helton [1981] Subinvariants for Analytic Mappings on Matrix Balls, *Analysis*, 1, pages 217–226.

[4] Ball, Joseph A. and J. William Helton [1982] Lie Groups Over the Field of Rational Functions, Signed Spectral Factorizations, Signed Interpolations, and Amplifier Design *Journal of Operator Theory*, 8, pages 19–65.

[5] Boyd, Stephen and Lieven Vandenberghe [1999] *Convex Optimization*, preprint from Stanford University.

[6] Das, Indraneel and J. E. Dennis [1998] Normal-Boundary Intersecting: A New Method for Generating the Pareto Surface in Nonlinear Multicriteria Optimization Problems, *SIAM Journal of Optimization*, 8(3), pages 631–657.

[7] Gonzalez, Guillermo [1997] *Microwave Transistor Amplifiers*, Second Edition, Prentice Hall, Upper Saddle River, NJ.

[8] Helton, J. W. [1972] The Characteristic Functions of Operator Theory and Electrical Network Realization, *Indiana University Mathematics Journal*, 22(5), pages 403–414.

[9] Helton, J. W. [1981] Broadbanding: Gain Equalization Directly from Data, *IEEE Transactions on Circuits and Systems*, CAS-28 (12), pages 1125–1137.

[10] Helton, J. W. [1982] Non-Euclidean Functional Analysis and Electronics, *Bulletin of the American Mathematical Society*, 7(1), pages 1–64.

[11] Helton, J. W. and O. Merino [1998] *Classical Control Using H^∞ Methods*, SIAM, Philadelphia, PA.

[12] Helton, J. W. and A. E. Vityaev [1997] Analytic Functions Optimizing Competing Constraints, *SIAM Journal of Mathematical Analysis*, 30(3), pages 749–767.

[13] Kim I. Y. and de Weck O. L. [2005] Adaptive Weighted-Sum Method for Bi-Objective Optimization: Pareto Front Generation, *Structural and Multidisciplinary Optimization*, 29(2), pages 149-158.

[14] Liu, L.C.T. and W. H. Ku [1984] Computer-Aided Synthesis of Lumped Lossy Matching Networks for Monolithic Microwave Integrated Circuits (MMIC's), *IEEE Transactions on Microwave Theory and Techniques*, MTT-32(3), pages 282–290.

[15] Newcomb, Robert W. [1962] *Linear Multiport Synthesis*, McGraw-Hill, New York, NY.

[16] Pozar, David M. [1998] *Microwave Engineering*, third edition, Prentice-Hall, Upper Saddle River, NJ.

[17] Schwartz, David F. and J. C. Allen [2004] Wideband Impedance Matching: H^∞ Performance Bounds, *IEEE Transactions on Circuits and Systems II: Express Briefs*, 51(7), pages 364–368.

[18] `www.Williamson-labs.com/attenuator.htm`

A Lossy Matching with Pads

Up to this point, the lossy part of the lossy matching 2-port consisted of a series resistor. This appendix offers a "case study" to further improve the lossy match of the LWC antenna.

The lossy part of the matching circuit is the "pad" highlighted in Figures A-1 and A-2. The shunt resistors usually have equal values ($R_1 = R_2$) while the series resistor is smaller than the shunt values. Such pads are commercially available to implement a variety of attenuations [16, pages 175–176]. Figures A-3, A-4, and A-5 show the action of selected pads on the Smith chart. In each figure, the shunt resistors are held to a constant value while the series resistor R_2 sweeps from 0 to 500 ohms. The plots show that the pads tends to contract and shift the Smith chart as R_2 increases.

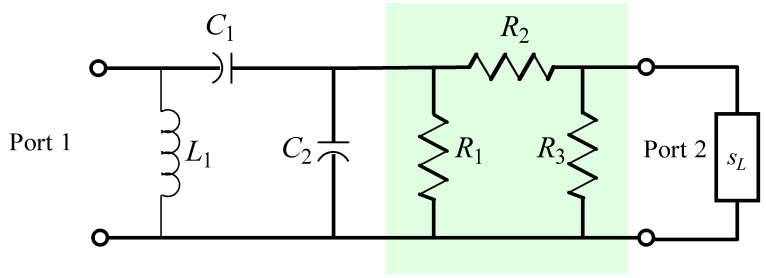

Figure A-1: Ladder and pad.

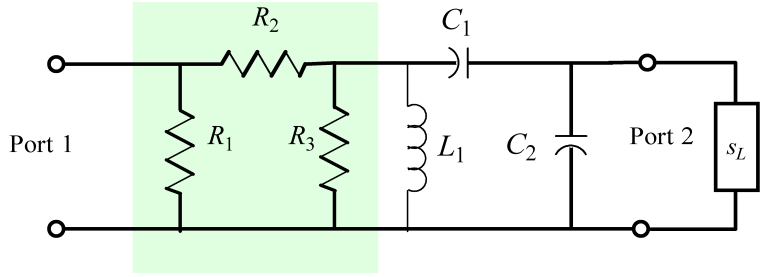

Figure A-2: Pad and ladder.

Motivation for using pads to match comes from the following observation: as the lossless matching network approaches the H^∞ bound, the input reflectance becomes circular in the Smith chart [17]. Given a circular reflectance, only a slight amount of attenuation will be needed to further pull the circle towards the origin. This appendix uses this observation to improve the lossy-matching tradeoff of Figure 18.

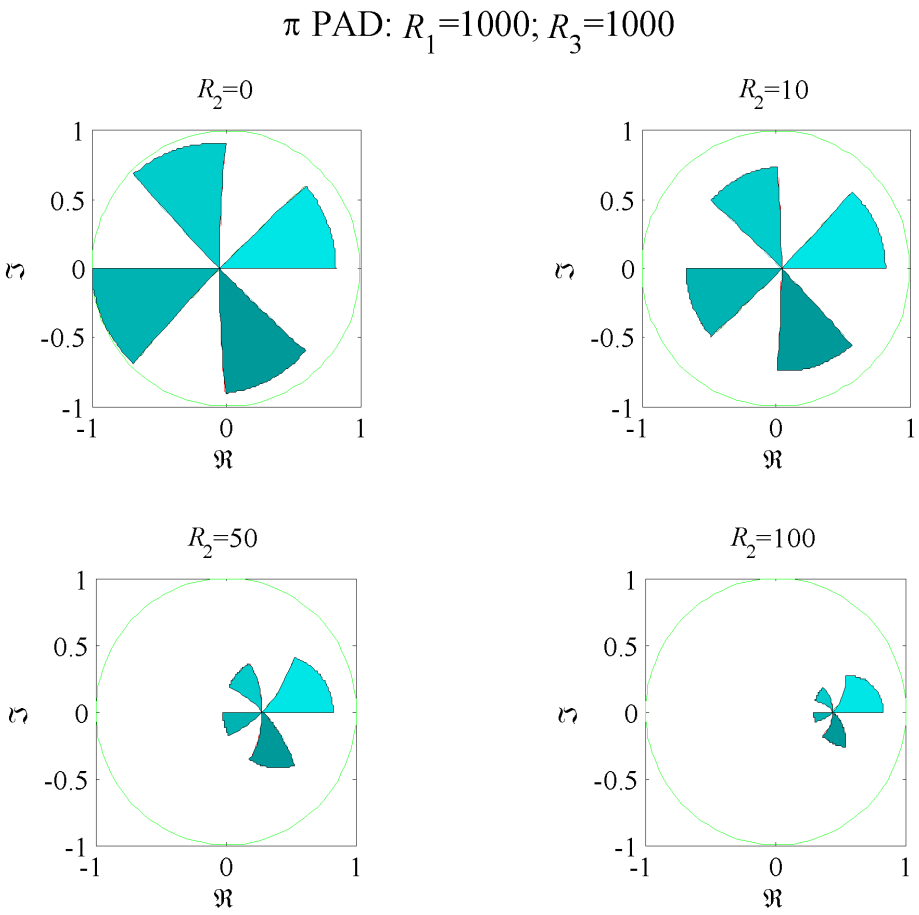

Figure A-3: The action of a 1000-ohm pad.

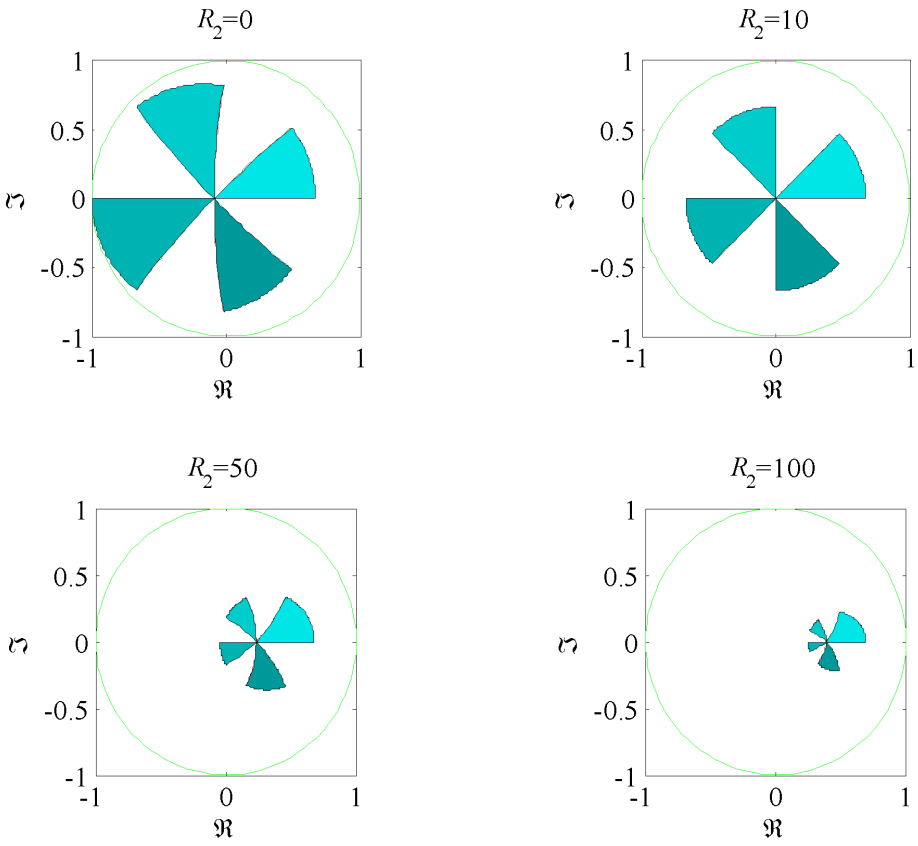

Figure A-4: The action of a 500-ohm pad.

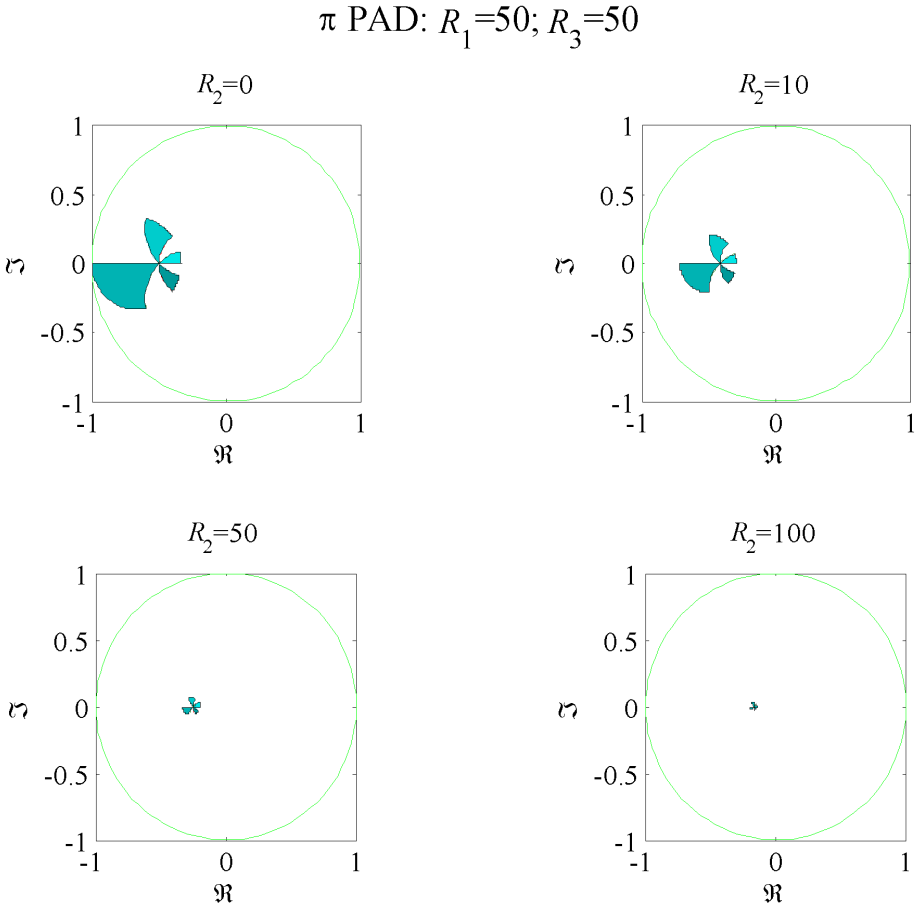

Figure A-5: The action of a 50-ohm pad.

Figure A-6 presents the matching delivered by the ladder-pad of Figure A-1. The blue dots mark random selections of the matching parameters. The reactive elements are bounded by Equation 9. The bounds on the pad's resistors are listed on the plot where R_1 need not equal R_3. The red boxes mark the minimal elements that are the starting points of the minimizer. The green diamonds mark an estimate of the Pareto front. Comparison with the series resistor of Figure 18 shows the pad offers little improvement in this configuration.

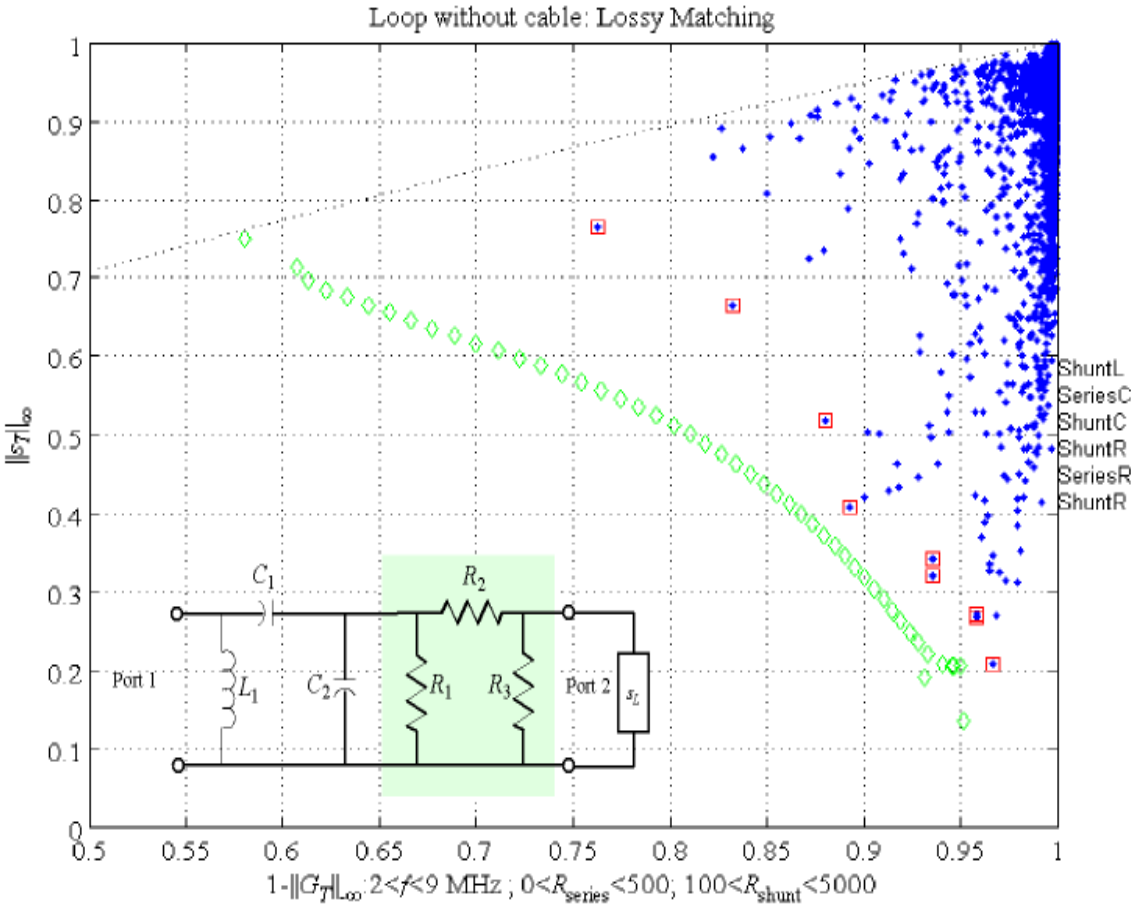

Figure A-6: Ladder-pad Pareto front estimate.

Reversing the order of the ladder and the pad leads to intriguing results. Figure A-7 shows the matching obtained from the pad-ladder of Figure A-2. The estimated Pareto front now shows that it is only an estimate. The figure shows families of local minima are trapping the minimizer.

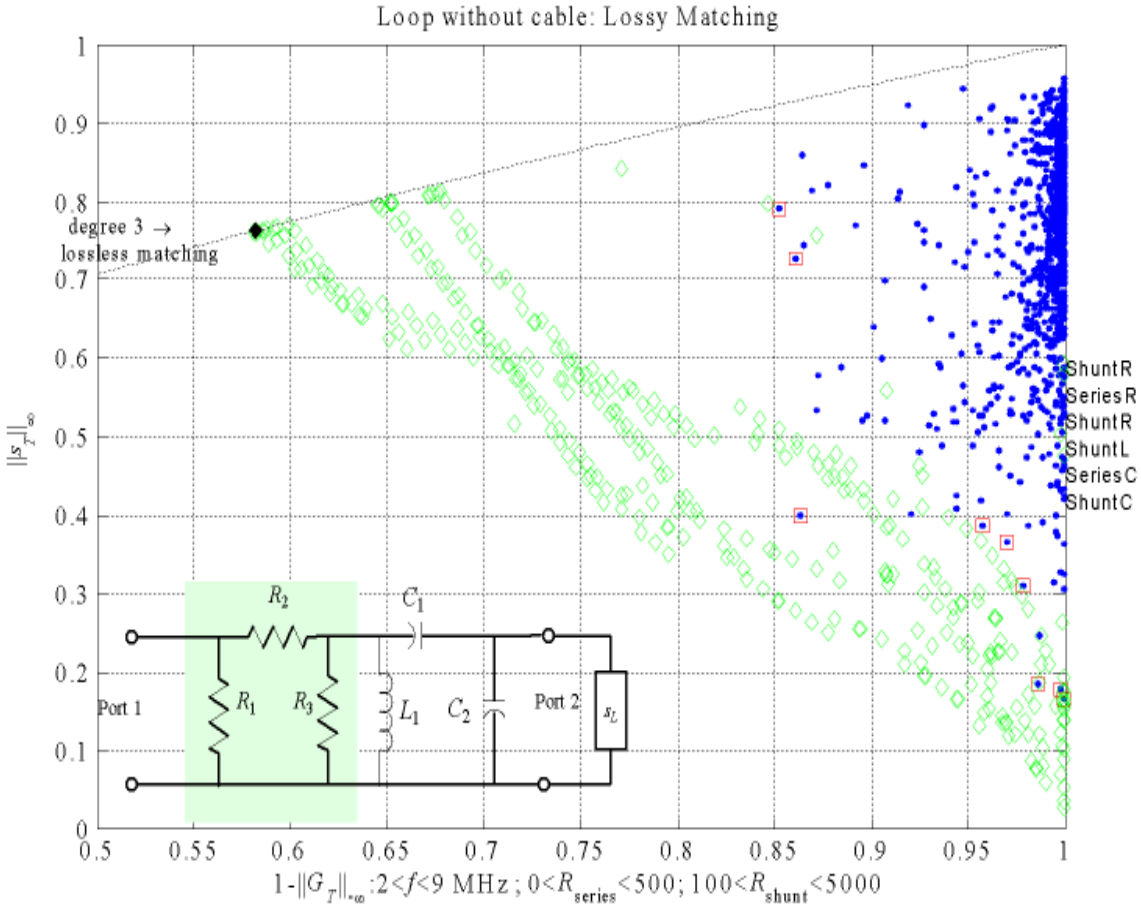

Figure A-7: Local minima of the pad-ladder.

Figure A-8 cleans up the preceding plot by applying a "Pareto filter" to better display the estimated Pareto front. Comparison with the ladder and pad Pareto front of Figure A-6 shows that both lossy matching circuits are similar near the lossless matching point. However, for decreasing input reflectance, the transducer power gain rolls off more slowly for the pad in

front of the ladder. For example, when the input reflectance is 0.4 or the VSWR is 2.33, the corresponding transducer power gains differ by almost 2 dB.

G_T (dB)	circuit
-8.8190	ladder and pad
-6.5686	pad and ladder

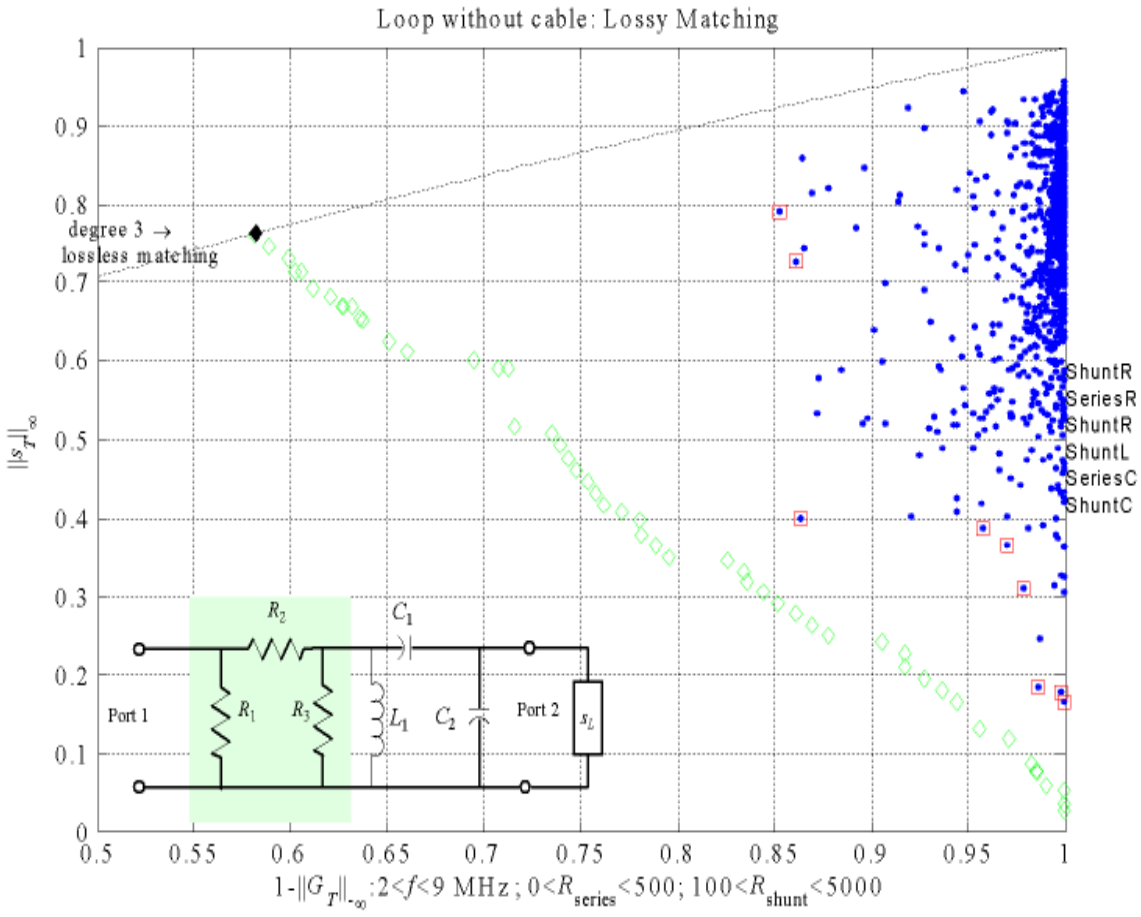

Figure A-8: Pad-ladder Pareto front estimate.

Figure A-9 explores the local minima structure by putting only a single series resistor in front of the ladder ($R_1, R_3 = \infty$). The performance is "messy" but comparable to the lossy matching circuit of Figure 18 that had the series resistor following the ladder. Thus, the shunt resistors of the pad are key to improving the tradeoff.

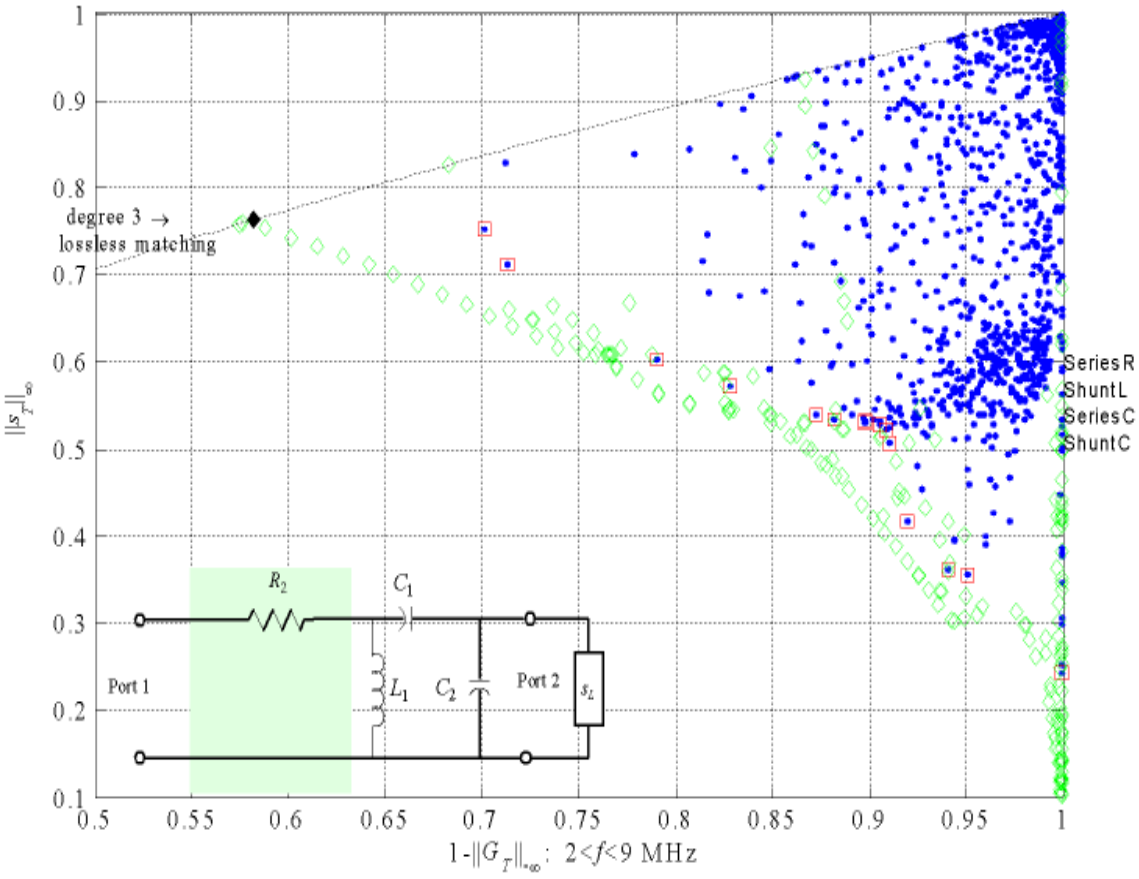

Figure A-9: Resistor-ladder Pareto front estimate.

Figure A-10 shows the effect of adding a shunt resistor to the preceeding matching circuit. The resulting lossy matching 2-port is a shunt-series resistor in front of the ladder ($R_3 = \infty$). This matching circuit obtains comparable performance as the full pad-ladder of Figure A-7 and delivers a better tradeoff than the lossy matching circuit of Figure 18.

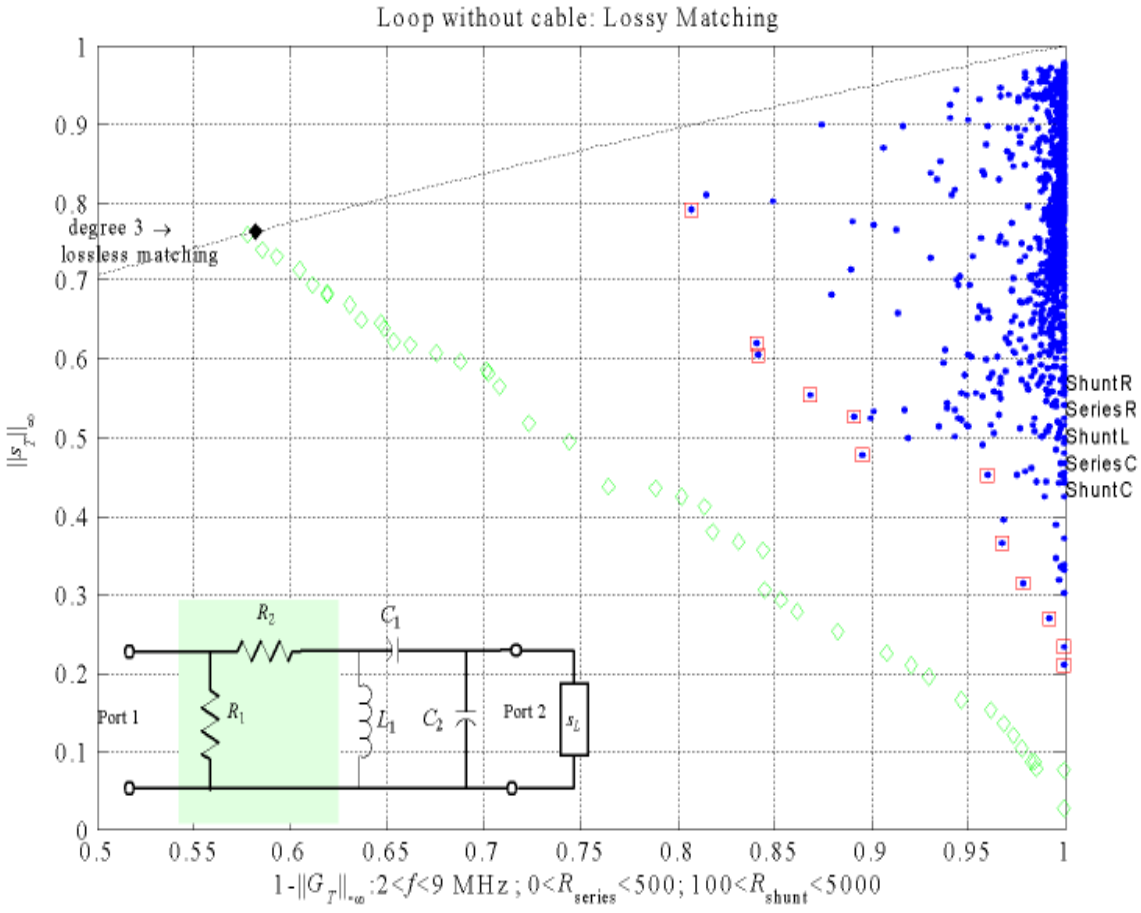

Figure A-10: L-ladder Pareto front estimate.

Thus, these relatively straightforward series of plots show how a circuit designer can step through the design process to iteratively improve the Pareto front or, equivalently, deliver an optimal lossy matching tradeoff.

Figure A-11 compares all the Pareto fronts in the engineering context. The plot shows the matching circuits split into two groups where the best performance in obtained by placing the attenuator in front of the lossless circuit as conjectured by Figure 29.

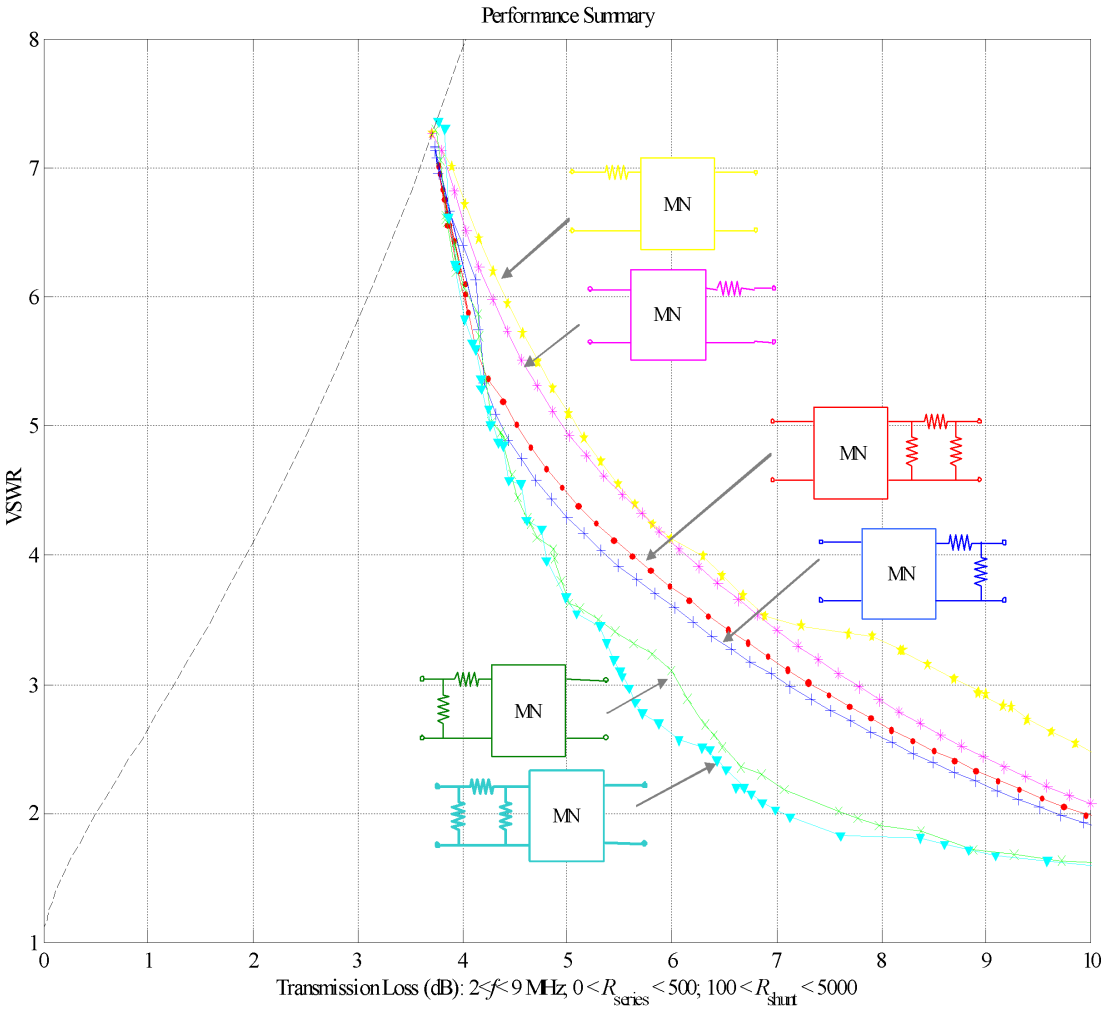

Figure A-11: Pad and ladder.

B Lossy Matching With π-Pads

This appendix continues the lossy matching "case studies" by specializing the π-pads used in the preceding appendix to attenuators. One attenuator design has the π-pad balance between equal impedances by setting the resistances as [18]

$$R_1 = z_0 \frac{K+1}{K-1}, \qquad R_2 = \frac{z_0}{2} \frac{K^2-1}{K}, \qquad R_3 = R_1, \qquad K = 10^{a/20},$$

where a denotes the attenuation in dB. This parameterization reveals the scattering matrix as

$$S_\pi = \frac{1}{K} \begin{bmatrix} 0 & 1 \\ 1 & 0 \end{bmatrix}.$$

The action of this scattering matrix S_π on reflectances s_L in the Smith chart is a contraction around the origin:

$$\mathcal{F}(S_\pi; s_L) = s_{\pi,11} + s_{\pi,12} s_L (1 - s_{\pi,22} s_L)^{-1} s_{\pi,21} = K^{-2} s_L \tag{B-1}$$

and is illustrated in Figure B-1.

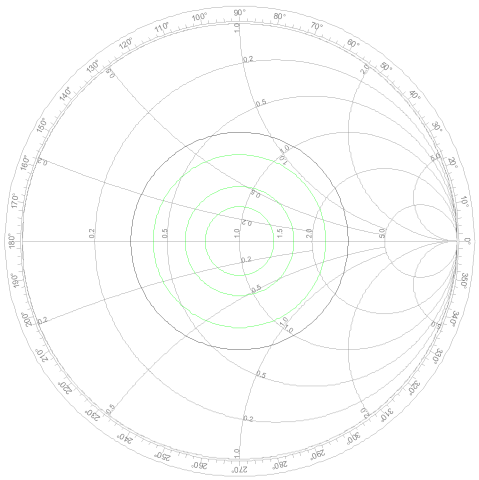

Figure B-1: π-pads contracting the circle $|s_L| = 0.5$ for $a = 1$, 3, 5 dB.

Figure B-2 shows the excellent matching obtained when this π-pad is placed in front of the lossless ladder. Figure B-3 shows the poor performance when the π-pad is placed after the lossless ladder.

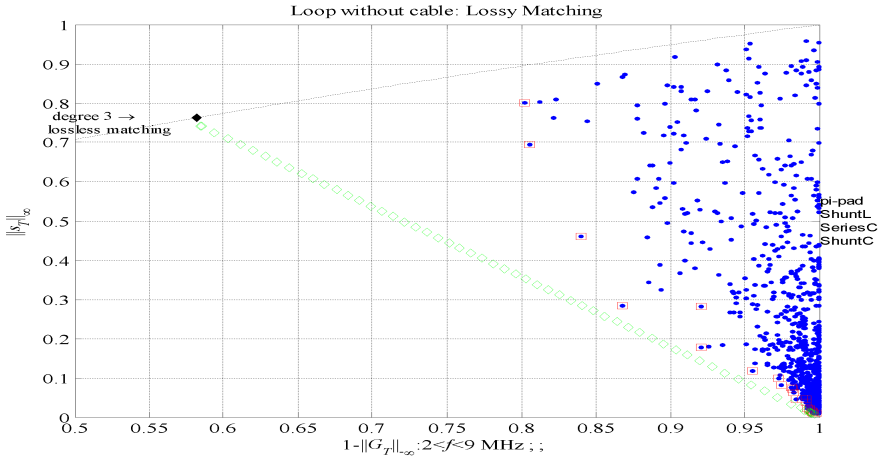

Figure B-2: π-ladder matching.

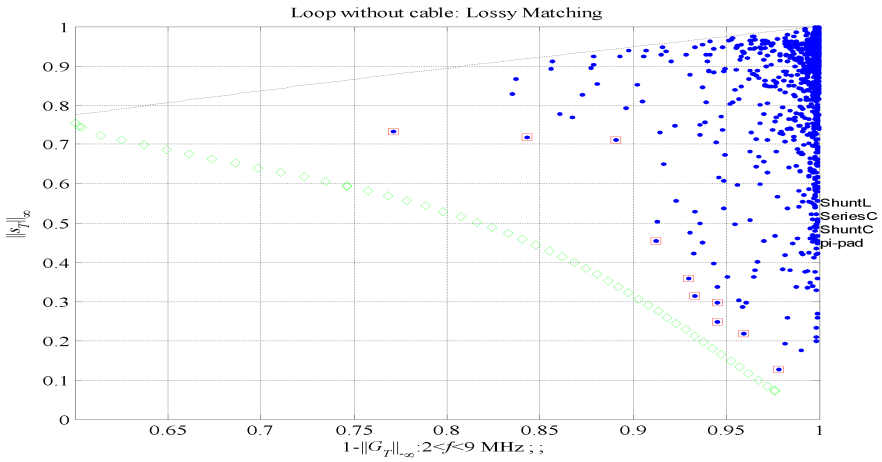

Figure B-3: ladder-π matching.

Figure B-4 compares the Pareto front of the π-ladder against the orbit of the ladder under the action of the π-pad. The orbit is computed by fixing the ladder and varying the pad.

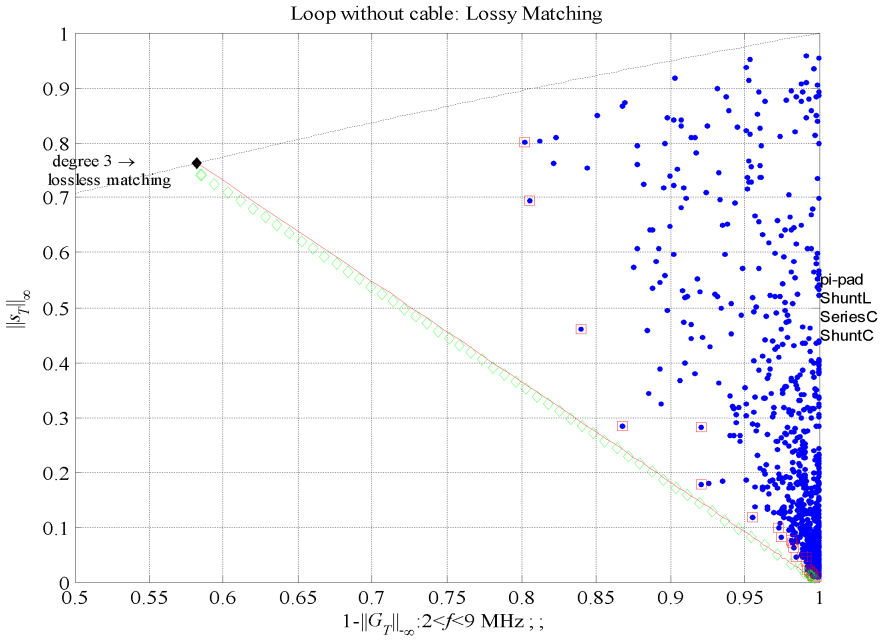

Figure B-4: The orbit of the π-pad.

The straightness and the close agreement of the orbit and the Pareto front are eye-catching and motivate the analysis of the performance function

$$\gamma = \begin{bmatrix} 1 - \|G_T\|_{-\infty} \\ \|s_1\|_\infty \end{bmatrix}$$

using the decomposition of Figure B-5. Let S_ℓ denote the scattering matrix of the ladder:

$$S_\ell = \begin{bmatrix} s_{\ell,11} & s_{\ell,12} \\ s_{\ell,21} & s_{\ell,22} \end{bmatrix}.$$

The reflectance at Port 1 of the ladder is

$$s_X = \mathcal{F}(S_\ell; s_L).$$

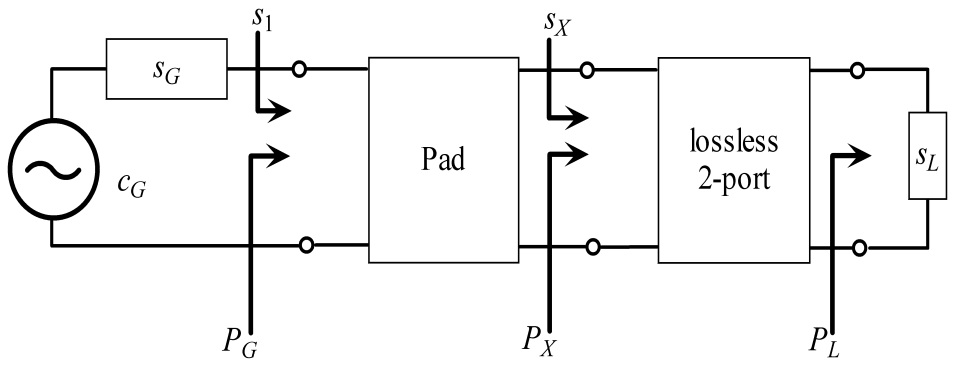

Figure B-5: Attenuator contracting the lossless matching.

The reflectance at Port 1 of the π-pad when s_X loads Port 2 follows from Equation B-1:

$$\|s_1\|_\infty = K^{-2}\|s_X\|_\infty. \tag{B-2}$$

The transducer power gain factors across the π-pad and the ladder:

$$G_T = \frac{P_L}{P_{G,\max}} = \frac{P_X}{P_{G,\max}}\frac{P_L}{P_X} = G_{T,\pi}G_P.$$

$G_{T,\pi}$ denotes the transducer power gain of the π-pad when Port 2 is loaded with s_X and Port 1 is loaded with a zero reflectance:

$$G_{T,\pi} = |s_{\pi,21}|^2 \left.\frac{(1-|s_G|^2)(1-|s_X|^2)}{|1-s_G s_1|^2|1-s_{\pi,22}s_X|^2}\right|_{s_G=0} = K^{-2}(1-|s_X|^2).$$

G_P denotes *power gain* G_P of the ladder [16, Eq. 11.8]:

$$G_P = \frac{|s_{\ell,21}|^2}{1-|s_X|^2}\ \frac{1-|s_L|^2}{|1-s_{\ell,22}s_L|^2}$$

Putting all the terms together yields

$$\begin{aligned} G_T &= K^{-2}(1-|s_X|^2)\frac{|s_{\ell,21}|^2}{1-|s_X|^2}\ \frac{1-|s_L|^2}{|1-s_{\ell,22}s_L|^2} \\ &= K^{-2}|s_{\ell,21}|^2\ \frac{1-|s_L|^2}{|1-s_{\ell,22}s_L|^2} \\ &= K^{-2}G_{T,\ell}. \end{aligned}$$

Cancelation turns the power gain of the ladder into the transducer power gain $G_{T,\ell}$ the ladder under the following *cancelation loading*:

- Port 2 is loaded with s_L;
- Port 1 is loaded with zero reflectance.

Taking the minium gives

$$\|G_T\|_{-\infty} = K^{-2} \|G_{T,\ell}\|_{-\infty}, \tag{B-3}$$

so that the attenuator and the lossless 2-port are essentially decoupled. Equation B-2 and B-3 show that the performance simplifies to

$$\gamma(K, S_\ell) = \begin{bmatrix} 1 - K^{-2} \|G_{T,\ell}\|_{-\infty} \\ K^{-2} \|s_X\|_\infty \end{bmatrix} = \begin{bmatrix} 1 \\ 0 \end{bmatrix} + K^{-2} \begin{bmatrix} -\|G_{T,\ell}\|_{-\infty} \\ \|s_X\|_\infty \end{bmatrix}.$$

Further simplification is possible using Equation 7. Because the ladder is lossless, the cancelation loading forces

$$\|G_{T,\ell}\|_{-\infty} = 1 - \|s_X\|_\infty^2.$$

Substitution gives

$$\gamma(K, S_\ell) = \begin{bmatrix} 1 \\ 0 \end{bmatrix} + K^{-2} \begin{bmatrix} \|s_X\|_\infty^2 - 1 \\ \|s_X\|_\infty \end{bmatrix}. \tag{B-4}$$

That is, the performance image of the π-pad and ladder is determined by the orbit of each element s_X under the action of the attenuator. Each such orbit is straight line starting on the lossless curve ($K = 1$) and traveling down to the lower right corner ($K = \infty$). Using a ladder is irrelevant. The only property of S_ℓ that is needed is that S_ℓ be lossless.

The preceding argument holds for any class of lossless 2-ports and can be summarized as follows:

Theorem 1 *Let $\mathcal{S}$ be any non-empty collection of 2×2 lossless scattering matrices. Assume the lossy matching circuit of Figure B-5. Assume $s_G = 0$. Denote the orbit of the load s_L under $\mathcal{S}$ by*

$$\mathcal{F}(\mathcal{S}; s_L) = \{\mathcal{F}(S; s_L) : S \in \mathcal{S}\}.$$

The performance image of this lossy matching family is

$$\gamma(\mathcal{S}) = \left\{ \begin{bmatrix} 1 \\ 0 \end{bmatrix} + u \begin{bmatrix} \|s_X\|_\infty^2 - 1 \\ \|s_X\|_\infty \end{bmatrix} : s_X \in \mathcal{F}(\mathcal{S}; s_L); u \in [0,1] \right\}.$$

The Pareto front of this performance image is the line segment

$$\gamma(u) = \begin{bmatrix} 1 \\ 0 \end{bmatrix} + u \begin{bmatrix} s_{\text{opt}}^2 - 1 \\ s_{\text{opt}} \end{bmatrix}; \quad (u \in [0,1]),$$

where s_{opt} is the smallest reflectance obtainable by lossless matching over $\mathcal{S}$:

$$s_{\text{opt}} = \inf\{\|s_X\|_\infty : s_X \in \mathcal{F}(\mathcal{S}; s_L)\}.$$

This result says that lossy matching can be done in two steps. First, undertake a lossless matching of the load. Second, take the best lossless match and use the attenuator to sweep out the Pareto front to "dial in" an acceptable gain–loss tradeoff.

Figure B-6 illustrates this theorem when the lossless matching family $\mathcal{S}$ produces reflectances $\|s_X\|_\infty = 0.5,\ 0.6,\ 0.7,\ 0.8,\ 0.9$. All but the smallest reflectance is plotted in blue. The smallest reflectance determines the Pareto front and is plotted in green.

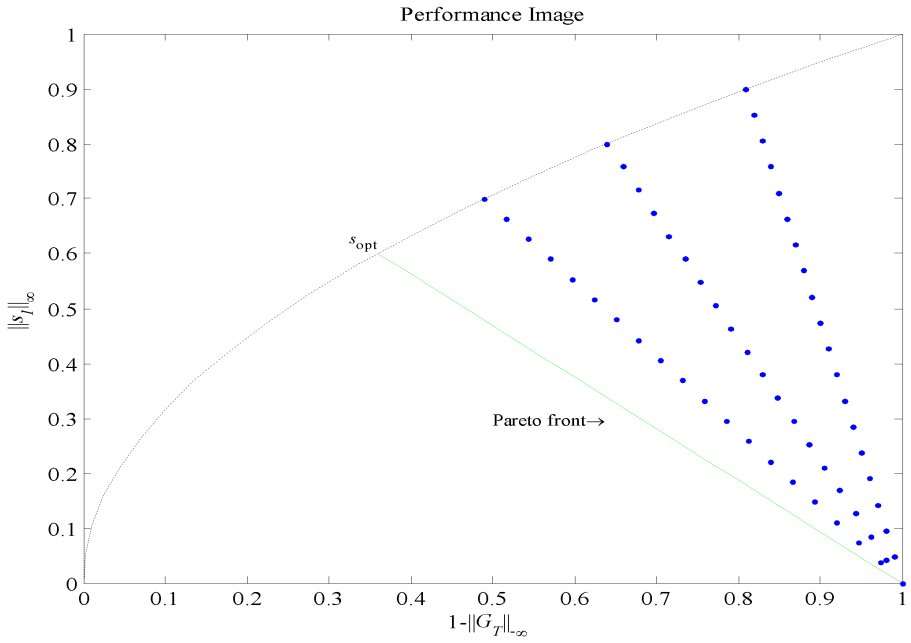

Figure B-6: Representative performance image and Pareto front.

When the H^∞ computation has produced the smallest reflectance attainable by any lossless 2-port, the resulting Pareto front is the hard design limit for lossy matching—assuming the topology of Figure B-5. Whether better performance can be obtained by different lossy matching topologies is an open question.